

Some Nonlinear Problems in Anisotropic Systems

P. E. Cladis and W. van Saarloos

4.1 Introduction

Although liquid crystals are nonlinear systems, their use to nonlinear science remains largely unexploited. A possible contributing factor is that the physics of liquid crystals has evolved over the past 10 to 15 years as a multi-disciplinary tributary to the main streams of physics, chemistry and biology. A special vocabulary has evolved to describe many of the physical properties of these systems. Frequently liquid crystal usage is at odds with main-stream usage, but, more often, it is a question of new words coined to describe liquid crystal properties that have no counterpart in other condensed systems.

Liquid crystals are new materials to technology so expertise in their handling and characterization has only recently advanced to the point where quantitative measurements are possible. Chemical purity can be measured in parts per 100. Defect free samples can be prepared. Sample geometry and temperatures can be controlled as never before. The dynamics and stability of structures possessing a wide variety of symmetries can be studied using liquid crystals. Symmetry does not change continuously but how it changes is a fundamental aspect of our understanding of the equilibrium and dynamical properties of phase transitions.

A unique feature of liquid crystals is that they are *soft systems* on a macroscopic scale. The direction of orientational order, the optic axis, can be successfully described by a continuum mechanics. Disclinations, the defects much studied in nematic phases, have no counterpart in solid systems. An as of yet, unexploited strength of these materials is that the creation, propagation and destruction of order can be studied in reduced dimensions. Equilibrium phases that theoretically exist in only two dimensions, such as the hexatic phase, can be studied with the aid of thin films. When well oriented, the smectic B to smectic A interface in directional solidification provides an example of a 2-dimensional (2-d) hexagonal crystal to 2-d isotropic fluid transition. The smectic A to isotropic interface, properly oriented, is useful to advance understanding of a 2-d liquid to 3-d liquid transition. The power of simplification is obvious.

Anisotropy usually plays a part in the propagation of order in liquid crystals and usually this is a complication. However, even in classical solid state, as exemplified by the latest rage in high T_c superconductors,¹ it is recognized that structural anisotropy may play a key role in creating materials with useful electronic properties. Fresh insights are needed² and these may be provided by visual observation of materials in the liquid crystal state. Even 3-d crystal transitions can be observed in these materials. For example, who can fail to be impressed by the naturalness, if not inevitability, of twinning when observing the *electric field* induced tetragonal to orthorhombic transition in blue phases in real time, in a polarizing microscope³?

Another unique feature of liquid crystals is that they provide qualitative solutions to complicated, often unsolvable, equations on a large scale that can be observed using a polarizing microscope. Once an answer is known, it is then sometimes possible to guess an approximate analytic solution. To a certain extent, they then play a role similar to numerical simulations of nonlinear equations.

Sometimes the answer is not easy to decode because it requires interpretation of complicated optical patterns. A useful strategy is, therefore, to prepare samples in simple geometries with well-defined boundary conditions. Although many solutions are lost, the few that can be interpreted feed one's intuition as to how solutions are selected. Another useful strategy has been to go to systems that have reduced dimensional order. Because the director can always escape into the third dimension in nematic⁴ (and cholesteric⁵) liquid crystal phases, introducing new instabilities, we have found it useful to investigate 2-*d* dynamical properties of anisotropic liquids by studying the dynamics of smectic C films: a 2-d anisotropic liquid in the plane of the film.⁶

In the past few years, our objective has been to seek quantitative answers to nonlinear problems from various liquid crystal systems. As mentioned above, quantitative information is not easy to obtain from these materials. Because of their nonlinearity, it is non-trivial to devise experiments where all factors are under control. In practice, this often implies that the size of the experimental cell has to be chosen with care. In cells that are too small, wall effects or other seemingly innocent experimental features may introduce perturbations that are magnified nonlinearly and so shroud important features of the problem. In cells that are too large, the nonlinear features are difficult to study since they cannot be properly localized.

In this chapter, we concentrate on those problems that one or both of us have been involved with over the years and that we believe have shown or will prove to be useful quantitative paradigms of nonlinear systems. Because of the limited scope of this chapter, we do not discuss in detail, but only list at the end, several recent developments where liquid crystals were used to investigate other outstanding problems in physics. Our point of view will be to use the physics of liquid crystals to give qualitative aspects of the solutions, and then discuss control parameters to develop a more quantitative picture. A quantitative picture is needed to serve as a guideline for future experimental and numerical work. A more ambitious aspiration is that familiarity with these results will inspire a deeper look at these and

similar problems, beautifully illustrated by materials in the liquid crystal state that may lead to a more fundamental understanding of nonlinear problems in general.

Here we interrupt the flow of "abstract ideas" to illustrate this point by telling the story of the oscillations in our own understanding. A detailed formal discussion and references can be found in a later section. We request our readers to take the unreferenced material in the next paragraph as unpublished private communications.

In 1981, while observing what they were told was a "ferroelectric" liquid crystal switching using a polarizing microscope, Cladis and Brand concluded that they were actually seeing walls moving. On dimensional grounds, they decided that switching times should scale as $(E)^{1/2}$ with E the applied field. In 1983, by including higher order terms in E , Cladis found an exact solution for a specific case that predicted that the speed was independent of E ! In 1986, van Saarloos showed that the $(E)^{1/2}$ dependence was also predicted by the new marginal stability idea. However, including higher order terms, marginal stability showed that the switching times would first increase, reach a maximum, then, decrease with increasing E . Finally, in 1988, we noticed that the maximum speed predicted by marginal stability corresponded to the speed predicted by the exact solution. Going back to the marginal stability arguments, it seems that "case II" marginal stability can be used to justify this result thus demonstrating the universality of marginal stability.

Even with this glimmer of understanding of a long-standing puzzle, the problem is still complicated. In the long term, however, we believe, it may prove a good example of how new ideas generated in nonlinear physics can be applied to observations made on liquid crystal materials, with profit to our understanding of both nonlinear physics and the material physics of complex materials.

Returning now to this chapter, the first two topics we discuss in section 4.2 are static problems. The next three addressed in section 4.3 are dynamic. Finally, we outline in section 4.4 problems that are particularly suited for nonlinear studies or that have recently been successfully investigated with liquid crystals.

4.2 Nonlinear Aspects of Static Properties of Liquid Crystals

The direction of long-range orientational order of liquid crystals can vary continuously over macroscopic length scales. This is one of their unique features: they are soft systems. This is illustrated in our first example where two forces, surface and electrostatic, compete to align the director. Electrostatic forces act uniformly throughout the bulk of the system but surface forces fall off exponentially with distance from the surface. Because the direction of orientational order is a unit vector, \mathbf{n} ($\|\mathbf{n}\| = 1$), the elastic energy of the simplest liquid crystal phase, the nematic phase, is nonlinear, even to lowest order. In order to minimize elastic and electrostatic contributions throughout its bulk, the director orientation varies spatially in a continuous but nonlinear fashion, with a soliton-like profile, above and applied threshold field.

Disclinations are a unique feature of soft systems. To describe these objects we consider two of the basic elastic deformations, called splay and bend, that these soft systems support without compromising long-range orientational order.

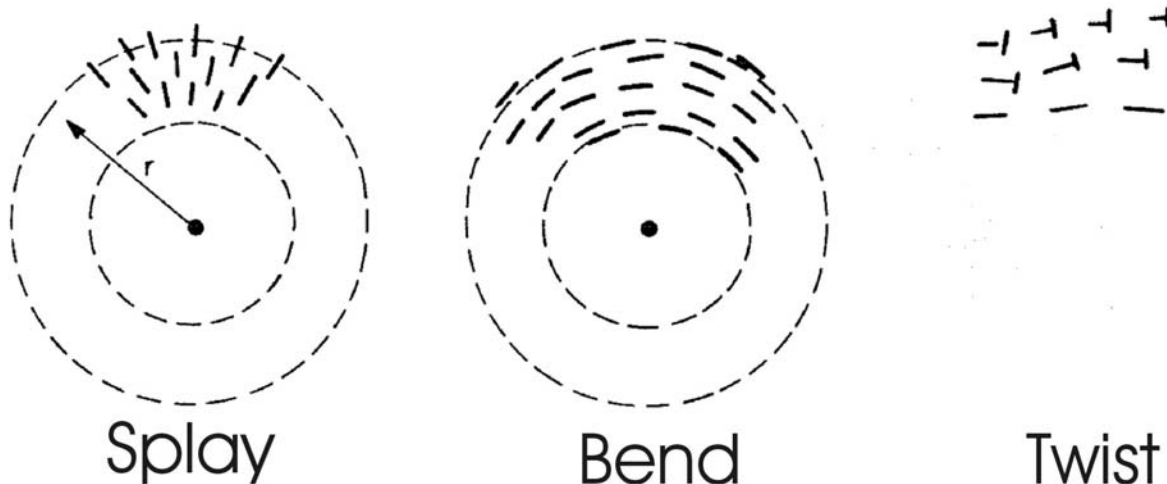


Fig. 4.1. In splay, n fans out as the spokes of a wheel whereas in bend, n follows the rim. In twist, n rotates about an axis perpendicular to n .

To describe splay it is useful to think in terms of the geometry of a wheel. In splay, n fans out as the spokes of a wheel. Fig. 4.1 shows this. The amount of energy required to create splay depends on how much the director is splayed. At a distance r from the axle, it requires an energy per unit volume, given by K_1/r^2 . It costs less energy the further the director is from the wheel axle. K_1 is called an *elastic constant* and its unit is a force. For nematic liquid crystals, the magnitude of K_1 is, typically, 5×10^{-12} newtons, a very small force. Bend deformation is also shown Fig. 4.1. In terms of the wheel geometry, instead of following the spokes, n follows the rim. K_3 is the elastic constant of bend. Its magnitude is about 7×10^{-12} newtons, or, a bit larger than K_1 but still small. Bend deformation often combines with splay in a splay-bend mode of deformation.

In the absence of external forces, an elastic deformation involving a rotation of n less than $\pi/2$ spontaneously relaxes to the uniform state to minimize the elastic energy. However, splay or bend deformation where n rotates an integral multiple of π radians *does not spontaneously relax*. It becomes an *object*, a quantized deformation called a *topological defect*. Line defects are called *disclinations* because, on a path around the line, n changes its *inclination* by $S \times 2\pi$, where, because of the symmetry $n = -n$, S can be $\pm 1/2, \pm 1, \pm 3/2 \dots$. The + sign refers to disclinations where the director rotates counter-clockwise around the defect line and the - sign, when it rotates clockwise. Fig. 4.2 shows examples of pure splay and pure bend disclinations for $S = +1/2$ and $S = -1/2$.

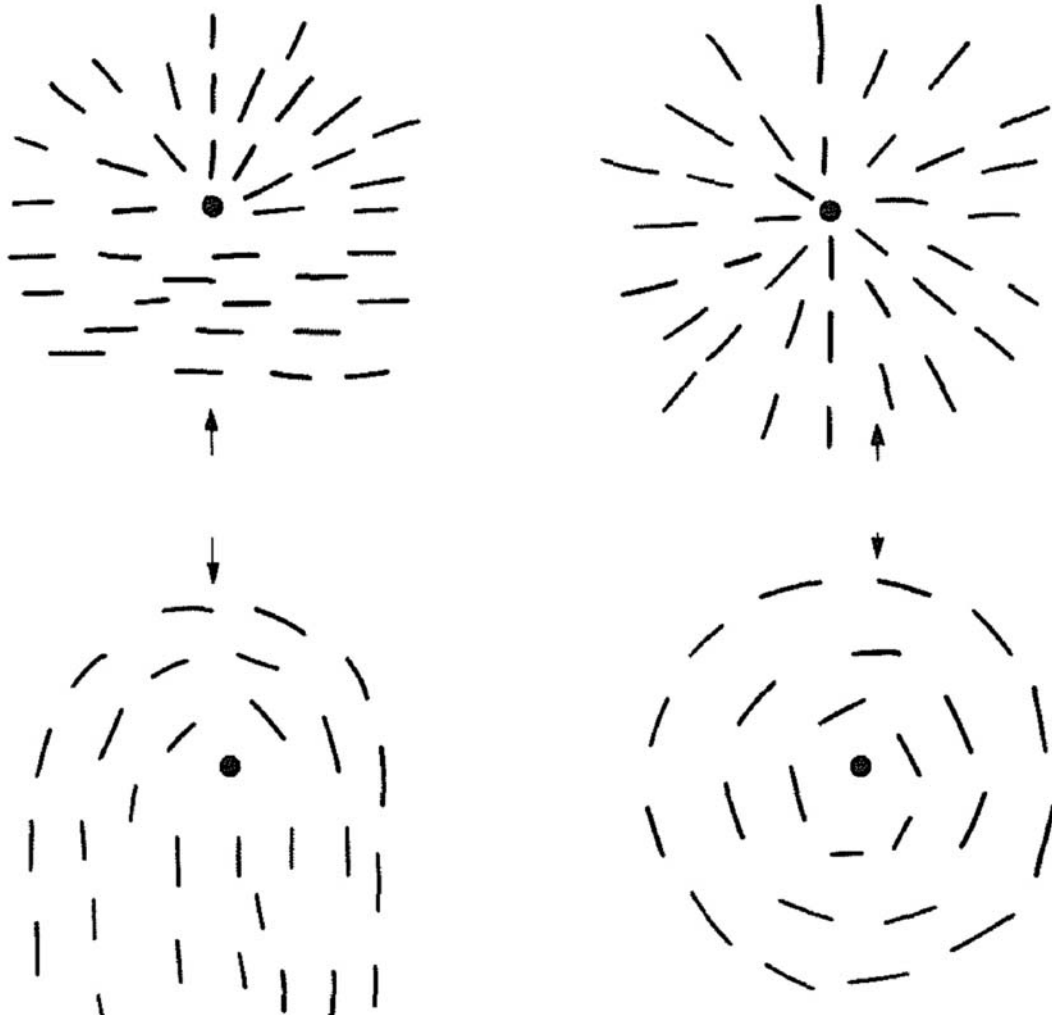


Fig. 4.2. Director pattern for splay and bend disclination lines.

Disclinations are fascinating objects. They are seen as either thick or thin threads floating in nematic liquid crystals. (Note that the name nematic is derived from "nema", the ancient Greek word for thread.) Fig. 4.3 shows an example of a "thin thread" along with a schematic of how the director is oriented around it.⁷ As the radius of the axle, r_c , shrinks, the elastic energy of the disclination increases like $\ln(r_c)$, to be infinite as $r_c \rightarrow 0$. A major step forward in our understanding of these systems was the discovery that, topology permitting, the director makes use of its nonlinearity by forming a soliton-like object as a minimum energy solution that satisfies the topological constraints imposed by boundary conditions. Before discussing an example of this behavior, we first discuss some aspects of the Freedericksz transition.

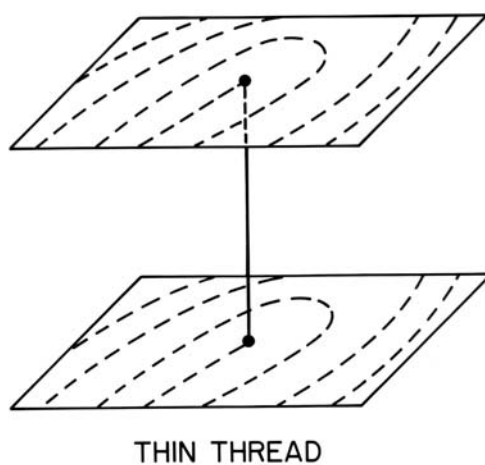


Fig. 4.3 The word nematic comes from the ancient Greek word for “thread”. This figure shows an example of a thin thread (Ref. 7). The thread is actually the core of an $S=1/2$ disclination line. The bottom figure is the director orientation around the thread.

4.2.1 Nonlinearities Associated with the Freedericksz Transition

One of the first equations encountered in the liquid crystal literature is the one describing the twist Freedericksz transition, a static sine-Gordon equation. To study the twist Freedericksz transition,⁸ the nematic liquid crystal is prepared between parallel glass plates so that in zero field, the director is uniformly oriented parallel to the plates. A magnetic (or electric) field is applied parallel to the plates but perpendicular to the director creating a torque to align \mathbf{n} parallel to \mathbf{H} . The Frank free energy has the form,

$$F = \frac{1}{2} \int_V dV \left[K_2 (\mathbf{n} \cdot \text{curl } \mathbf{n})^2 - \chi_a (\mathbf{n} \cdot \mathbf{H})^2 \right], \quad (4.1)$$

$K_2 \approx 2 \times 10^7$ dynes is the elastic constant of twist, $\chi_a \approx 1 \times 10^7$ cgs units is the diamagnetic anisotropy, $\chi_{\parallel} - \chi_{\perp}$ where \parallel and \perp are relative to the director, \mathbf{n} . In a Cartesian system of coordinates with z perpendicular to the glass plates, x parallel to \mathbf{n} at $z = \pm d/2$ and y parallel to \mathbf{H} , the Euler-Lagrange equation can be written in the form:

$$K_2 \frac{d^2 2\phi}{dz^2} + \chi_a H^2 \sin 2\phi = 0, \quad (4.2)$$

where ϕ , the angle measuring the deviation of \mathbf{n} from its zero field value, is a function of z only.

Surface forces constrain \mathbf{n} for all values of the applied field but their strength falls off exponentially with distance from the surface. Although, the orientation on the top and bottom surfaces, $z = \pm d/2$, is determined by surface forces, the orientation of \mathbf{n} at $z = 0$ is determined by a competition between surface and electrostatic forces. When the surface force wins, \mathbf{n} is constant throughout the sample. Eventually with increasing field strength, the strength of the electrostatic force is sufficient to first balance, then, overcome the surface forces and the orientation at $z = 0$ starts to change to gain magnetic energy for the system.

A first integral of Eq. 4.2 can be obtained by multiplying through by the integrating factor $d\phi/dz$. The condition that $d\phi/dz = 0$ in the middle of the sample, $z = 0$, where $\phi = \phi_m$, the maximum value of ϕ , then determines the resulting constant of integration for the non-trivial solution. In the final integration, leading to the complete elliptic function solution for the director configuration throughout the nematic slab, the second boundary condition, $\phi = 0$ at $z = \pm d/2$ is used, where d is the sample thickness.

It is convenient to compare lengths to the magnetic coherence length, ξ , $\xi = (K_2/\chi_a H^2)^{1/2}$. The condition that the non-trivial solution exists is $\xi = d / \pi$. The equality defines a critical field, H_c . For $H < H_c$, the relevant lowest energy solution is the homogeneous solution, $\phi = 0$ for all z . Experimentally then, as the field increases, ϕ remains zero until the threshold field is

achieved and then, ϕ departs from zero in the center of the sample. This departure can be sensitively observed by viewing the sample along the z-axis in convergent, monochromatic light.⁸ The value of H_c , thus gives a measure of the ratio of the material constants, K_2/χ_a .

If a field, $H \gg H_c$ is applied to initialize $\phi_m \neq 0$, then, when the field is switched off, ϕ_m decays exponentially to zero with a time constant, γ_1/χ_a . This can be seen by equating the right hand side of Eq. 4.2 with $H = 0$, to $\gamma_1 (\partial\phi/\partial t)$. This is a simple way to measure one of the important dynamical constants characterizing director relaxation in the elastic field⁸ in a linear dynamic limit. Recently, Kamenskii⁹ has discussed the nonlinear dynamics of twist deformations for nematic liquid crystals. While many of the effects he describes may be difficult to pin down in nematic liquid crystals, materials well oriented in the smectic C phase may prove useful to test some of his ideas.

4.2.2 Escape into the Third Dimension

Constraining a nematic in a long cylinder so that the director has only a radial component (perpendicular to the cylinder axis) results in a splay deformation whose associated energy has a logarithmic divergence as $r \rightarrow 0$, r being the distance from the cylinder axis. This requires the introduction of a core region where the approximation of first order elasticity breaks down. Similarly, if the director has only an azimuthal component in the plane, the bend energy is infinite at $r = 0$. But, relaxing the planar constraint by allowing the director to develop a z-component as a function of r , results in an elastic energy that is everywhere finite.

To illustrate this point, we write the director in cylindrical coordinates,⁴ $n_r = \cos\Phi(r)$, $n_\phi = 0$ and $n_z = \sin\Phi(r)$, and assume all elastic constants to be equal, $K_1 = K_2 = K_3$. On the boundary, $r = R$, $n_r = 1$ and $n_\phi = n_z = 0$.

Neglecting boundary terms, the Frank free energy becomes here:

$$F = \frac{K}{2} \int_0^R dr \left[\frac{\cos^2 \Phi}{r} + r \left(\frac{d\Phi}{dr} \right)^2 \right]. \quad (4.3)$$

The Euler-Lagrange equation then becomes simply,

$$\frac{d}{dr} \left(r \frac{d\Phi}{dr} \right) = - \frac{\sin \Phi \cos \Phi}{r}. \quad (4.4)$$

The trivial planar solution, $\Phi = 0$, exists indicating that it also is an extremum of the elastic energy. The first integral to Eq. 4.4 is:

$$\left(r \frac{d\Phi}{dr} \right)^2 = A^2 - \sin^2 \Phi, \quad (4.5)$$

where A is the constant of integration. The constant of integration is found by using Eq. 4. 5 to transform the integral of Eq. 4.3 then differentiating with respect to A. The minimum energy solution is then easily found to be $A = 1$ so that:

$$\frac{r}{R} = \cot \left(\frac{\pi}{4} + \frac{\Phi}{2} \right) \quad \text{for } 0 \leq \Phi \leq \frac{\pi}{2} \quad (4.6)$$

OR

$$\frac{R}{r} = \cot \left(\frac{\pi}{4} + \frac{\Phi}{2} \right) \quad \text{for } 0 \geq \Phi \geq -\frac{\pi}{2}, \quad (4.7)$$

a static soliton. Thus, the minimum energy solution is the one where the director is oriented radially near the walls and in the plus or minus z direction in the center.

This is a remarkable result.⁴ Without imposing symmetry breaking from the boundary condition, a nematic liquid crystal in a capillary self-organizes itself by escaping into the third dimension thereby spontaneously breaking the symmetry. The system finds a nonlinear solution to the old problem of minimizing the total energy. By making use of its nonlinearity in an original and unexpected way it finds a configuration with finite energy. Recently, Almgren and Lieb have proven deep theorems on the spontaneous symmetry breaking inherent in nonlinear systems such as this case in nematic liquid crystals.¹⁰

The theoretical result, Eq. 4.6, can be checked by simple observations.¹¹ A capillary tube is first prepared to enforce the boundary condition $n_r = 1$ at $r = R$. After filling with any nematic liquid crystal, the capillary is then surrounded externally by an index-matching compound to avoid optical effects from its cylindrical shape. The experimental technique used to show the director orientation in a plane that contains a diameter of the capillary, was to illuminate the sample through a regular array of small holes such as provided by spatial filters.¹¹ Because the liquid crystal is birefringent, each small spot of light gives an ordinary (seen as faint dots) and an extraordinary image (seen as brighter dots) displaced with respect to each other in the direction of the tilt of the optic axis (i.e. \mathbf{n}). The inclination of the displacement can be measured as a function of r/R and compared to a theoretically computed value. Reasonable agreement can be obtained even without correcting for the complicated optical geometry. Qualitatively, therefore, the effect exists.

Point Defects

By making these simple observations, point defects were discovered for the first time.¹¹ Line defects, the disclinations, were known. In thin nematic films, it was understood that an infinitely short line defect was a point defect in 2 dimensions. The point defects here are point

defects in the bulk. They arise because of the two equivalent directions for escape into the third dimension. They are observed along the capillary axis and are of two types with different elastic energies¹ that alternate along the axis (Fig. 4.4). If two neighboring points are far from each other they exist as stable states in "**asymptotic freedom**".⁷ Close together, their elastic fields interact attractively. They then move rapidly towards each other *at different speeds* and annihilation, leaving no trace [see footnote 1]. Work on the dynamics of such defects has only recently started.¹²

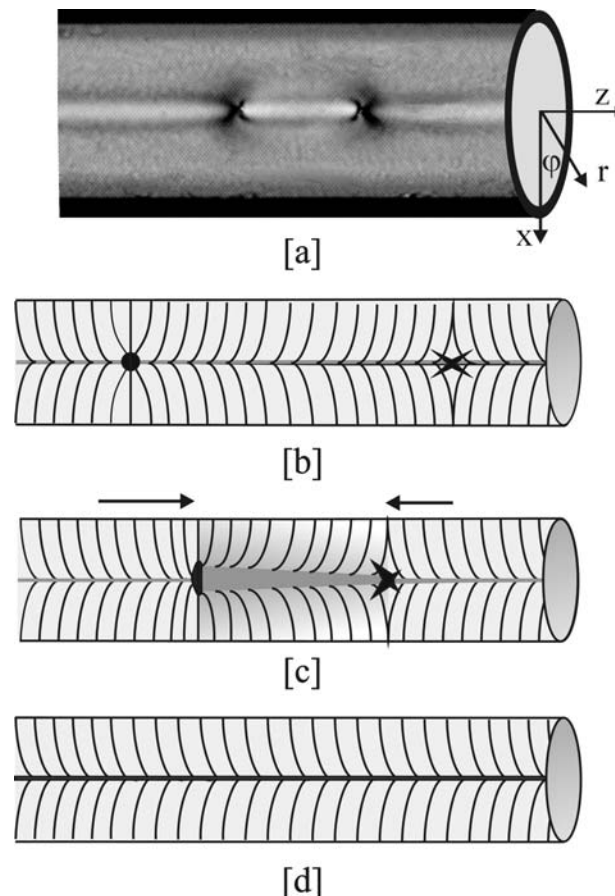


Fig. 4.4 Updated and replaced with Fig. 1 from P.E. Cladis and H.R. Brand, [Hedgehog-antihedgehog pair annihilation to a static soliton](#), *Physica A*326, 322 (2003).

Anisotropy of Elastic Constants

If a material is chosen with a nearly second order nematic-smectic A transition, the elastic constant of bend becomes large as a function of temperature near the transition temperature to the smectic A phase. The director "escape" is thus confined to a smaller and smaller region about $r = 0$ of the capillary.¹³ Eventually a pure splay $S = 1$ defect is formed in the smectic A phase. Upon reheating to the nematic phase, the $S = 1$ defect spontaneously breaks into two S

¹ From: Cladis and Brand, *Physica A*326, 322 (2003): the energy/length of a static soliton in units of K is $E_{SS}/\pi K = 2$. That of the hedgehog is $E_H/\pi K = 8$ and that of the antihedgehog is $E_{AH}/\pi K = 3$. While the hedgehog energy per length is larger than that of the static soliton, that of the antihedgehog is closer to that of the static soliton and 1/3 that of the hedgehog.

= 1/2 defect lines. Point defects are required to mediate the transition from the planar solution to the lower energy "escaped" solution.

4.3 Nonlinear Macroscopic Dynamics of Liquid Crystals

In the previous section, we have seen that the equation describing the static director profile in the Freedericksz transition obeys an equation similar to the static sine-Gordon equation. The sine-Gordon equation, $\Phi_{tt} - c^2 \Phi_{zz} = m^2 \sin \Phi$, is, of course, one of the basic equations that admits soliton solutions; one might therefore naively expect that recent progress in the field of soliton dynamics must have been as important to dynamical studies in liquid crystal, as it has been to other fields in physics.¹⁴

This is not true, however. The reason is that a soliton picture is, strictly speaking, only a good starting point for physical systems where elementary or wall-like excitations can move nearly freely, *i.e.* without appreciable damping. Liquid crystals, however, are visco-elastic, so that the dynamics of deformations or wall-like excitations is damped and subject to increasing elastic forces as when, for example, boundaries are approached. To illustrate this point, let us consider a sine-Gordon equation with a phenomenological damping term, $\gamma\dot{\phi}$, included¹⁵.

$$I \frac{\partial^2 \phi}{\partial t^2} + \gamma \frac{\partial \phi}{\partial t} - c^2 \frac{\partial^2 \phi}{\partial z^2} = m^2 \sin \phi . \quad (4.8)$$

This equation with γ small is a reasonable starting point to study the motion of magnetic walls, and similar equations have been used to describe a variety of other physical phenomena. In the absence of friction, soliton solutions with a whole range of velocities exist, and consequently, the low temperature spin dynamics of certain magnetic chains can be understood in terms of a dilute gas of such solitons with a distribution of velocities.¹⁴

In liquid crystals, on the other hand, the damping term $\gamma\dot{\phi}$ is believed to be large compared to the second order time derivative ϕ_{tt} whose magnitude is controlled by a moment of inertia, I . Although, the magnitude of I is unknown (it has so far not been measured), it is often taken to be related to the moment of inertia of a single molecule making this term negligibly small. Kamenskii⁹ argues that this choice for I is not an obvious one for liquid crystals, and suggests some experiments for measuring it. Furthermore, he makes the important point that macroscopic descriptions like hydrodynamics and director theories, presuppose averaging over a physically small volume but one that, nevertheless, contains many molecules. His point may be particularly relevant for lyotropic liquid crystals where the microscopic structure is one of large molecular aggregates. However, in this chapter, we will suppose that although the moment of inertia is much larger than that of a single molecule, it is nonetheless small relative to the friction term.

After a redefinition of the constants, Eq. (4.2), therefore, becomes of the type

$$\gamma \frac{\partial \phi}{\partial t} = K_2 \frac{\partial^2 \phi}{\partial z^2} + \frac{1}{2} \chi_a H^2 \sin 2\phi, \quad (4.9)$$

the generalization of Eq. (4. 2) for the director angle to the time-dependent case. From its form, it is seen that the time dependence of ϕ is determined by a simple balance between a friction term and the energy gain that provides the driving force.

In comparison with soliton systems ($\gamma \rightarrow 0$), we physically expect the following qualitative behavior in the large damping regime relevant for liquid crystals:

- i. With large friction, freely propagating wall-like solutions cannot persist - they mainly occur either when energy is constantly being pumped into the system, as, for example, in the study of Brochard et al.¹⁶ where the sample rotates in a magnetic field, or as a transient behavior after the system is suddenly brought into a metastable or unstable state (e.g., by switching an electric field - see section 4.3.2). Clearly, walls or fronts in liquid crystals will not have the property usually associated with the definition of a soliton: two solitons can maintain their shape following interactions or collisions with each other. In liquid crystals, this does not usually happen owing to the collapse or build up of elastic fields involved in their interactions.
- ii. One intuitively expects any front created in a liquid crystal to relax quickly to some asymptotic speed, c , independent of the details of the initial conditions, since this is typical for systems with large dissipation. Indeed, in section 4.3.2, we present one such example where this is the case because the friction term is balanced by a driving force and the front profile is maintained by a potential term.

The above discussion clearly demonstrates that the nonlinear behavior of liquid crystals is an interesting subject in its own right, because similarities with solitons occur on the static level while important differences usually manifest themselves on the dynamic level.

As we shall discuss, in most cases of moving defects or of interfaces (walls) where a stable state propagates into a region of space formerly occupied by a metastable state, the velocity can be determined from a simple balance of the energy of dissipation and the energy gain that provides the driving force e.g. Eq. 4.9. The physics of fronts propagating into an unstable state is somewhat different, though. Fortunately, in the last decade the dynamics of such fronts has been studied in detail mathematically as well as physically.¹⁷ As it turns out, the asymptotic velocity, c , referred to above is then determined by a simple dynamical mechanism, often called ‘marginal stability’.¹⁷ These results have only recently been applied to liquid crystals.

In passing, we note that the equations describing fronts propagating into unstable states in liquid crystals are closely related to those often used to model nerve pulse propagation.¹⁸ This is just one of many points of contact between the field of liquid crystals and biophysics.

The first two examples discussed in this section illustrate the above considerations. In our first example, an experiment is performed where a topological line defect ($S = -1/2$) is forced to move with constant speed c under the action of an applied voltage V . In line with the discussion above, we show that the line speed is determined by a competition between the viscous damping and the free energy the system gains by displacing the line. The problem is analogous to that of a solid body falling through a viscous medium in a constant force field with an important difference. We then describe an experiment where walls are created that propagate into an unstable state, and discuss how to determine the velocity in such a case.

Velocity gradients exert torques on \mathbf{n} . As will be seen in our third example, complications escalate with the addition of velocity gradients motivating a drive to even simpler geometries and dimensions. In our last example, we discuss flow in freely suspended smectic C films, where the director is confined to the two dimensions of the film. Even with this simplification, the problem is still rich in effects.

4.3.1 Dynamics of Line Defects in Nematic Liquid Crystals

To study the defect dynamics under controlled conditions (without being affected by walls), the induced deformations have to be confined to a localized region away from the walls; this can be done with the aid of external fields. In the experiment considered here,¹⁹ a line defect is created whose excess energy is linearly proportional to its distance from one of the walls; we study its motion and show that it rapidly approaches a constant speed, as expected from elementary considerations. Although the propagation of a line is physically different from domain walls, its speed is again determined by the competition between the free energy gained by displacing the line and viscous damping hindering its motion¹⁶.

Fig. 4.5(a) shows the experimental set-up. The nematic liquid crystal, 5CB, (cyano-pentyl biphenyl), is sandwiched between two transparent InO electrodes separated by wire spacers. The wires are electrically insulated from the InO surfaces by a thin coating of varnish. All surfaces are treated so that director orientation is perpendicular to them.²⁰ These boundary conditions force the director to form $S = -1/2$ line defects parallel to the wires in the mid-plane of the sample. The sample thickness, $2h$, is $140\mu\text{m}$, determined by the wire thickness, and the distance between the two wires is $\sim 1\text{mm}$. The experiment is to apply a 1 kHz a.c. voltage, $V_h = 90$ volts, between the two wires forcing the line to move away from the wire (Fig. 4.5b) since the dielectric anisotropy, ϵ_a of 5CB is positive, $\epsilon_a \approx 1$. Eventually the line comes to rest a distance, ℓ , from the wire. V_h is then turned off and simultaneously (within $50\mu\text{s}$), a vertical voltage, V_v , is applied to the InO electrodes forcing the line to move back towards the wire ($\ell > 0$) with a speed, c . The experiment is filmed with a video camera and the motion of the line analyzed.

As soon as V_v is turned on, a wave of director re-orientation moves through the material without displacing the line. This is interpreted as a readjustment of the director pattern, shown in Fig. 4.5(c), to one where the vertical distortion is now localized in the middle of the sample.

After this, the line defects start to move towards the wire. The first reorientation wave is fast (milliseconds)²¹ compared to the motion of the line defect (seconds).

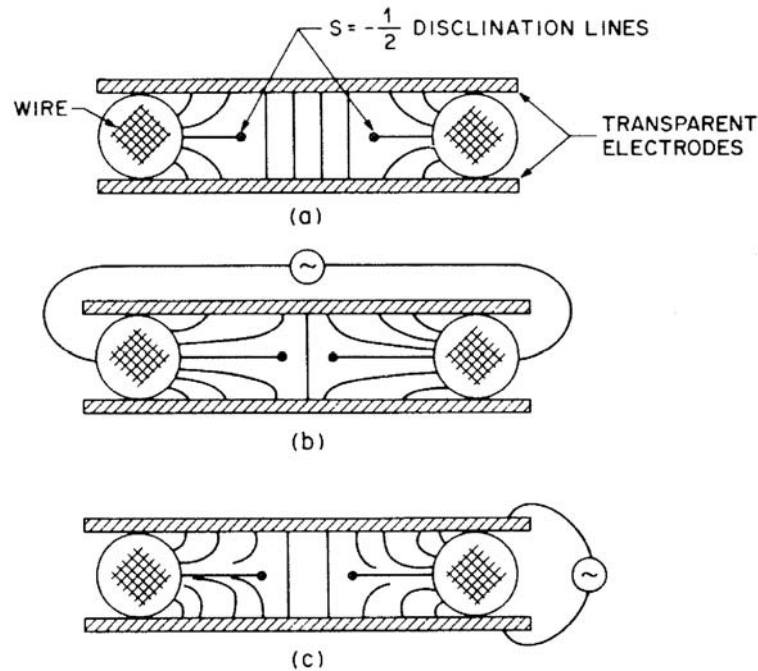


Fig. 4.5. (a) The experimental geometry: $V_h = V_v = 0$. (b) The lines move to the center of the sample when V_h is turned on. (c) The director pattern immediately after $V_h \rightarrow 0$ and V_v is turned on.

The importance of this first wave is that it sets up a *stable* but more energetic director configuration on the wire side of each line. Physically, if the center of the line is at $y = 0$, then for $y > 0$, the director wants to turn one way and for $y < 0$, the other way. For concreteness, consider the left defect. The only way the less energetic configuration can replace the more energetic splay-bend distortion of the director, is by moving the line to the left. While the region to the right is absolutely stable²² the region to the left is *metastable*. The line defect can thus be viewed as an energy barrier that has to be overcome before the total energy can be reduced by replacing the metastable state with the absolutely stable state. The physics is therefore different from that of the motion of a wall separating an unstable state from a stable state.

Contrary to the case of the interaction of two defects in the absence of fields, the electric field in this experiment confines the distortion of the director to a thin region around $y = 0$. This results in an excess energy for the line that is linear in the distance ℓ from the wall, and implies a constant force on the line. As discussed in more detail below, we then expect the line speed to approach a constant value c whose voltage dependence is determined by the change in excess energy with voltage. This is borne out by the experiments.

A few milliseconds after applying V_v , the line starts to move towards the wire and is tracked over a distance of about $200\mu\text{m}$ from the beginning of its motion until it comes to rest close to the wire. Fig. 4.6a shows the variation of c with applied voltage at 32°C . Except for the region, $V \sim 0$, c is proportional to the applied voltage. A linear least squares fit to the data

gives the constant of proportionality, $\beta = 4.7\mu\text{m/volt-sec}$. Fig. 4.6b shows β as a function of temperature. The data is shown as points.

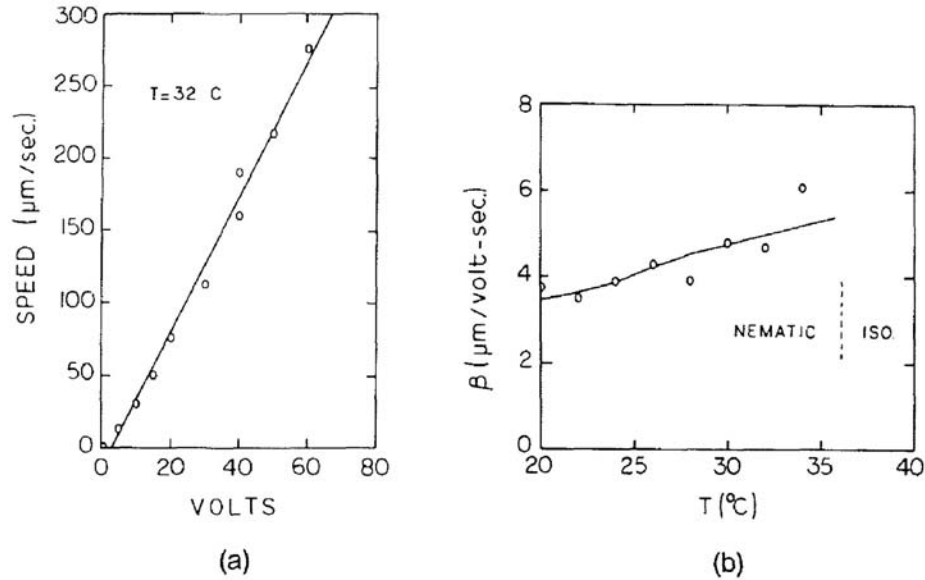


Fig. 4.6 Characteristics of the line motion. (a) The line speed is linear in V_v with slope β . (b) β as a function of temperature for 5CB for which the nematic to isotropic transition temperature is 36°C from Ref. 19.

Using the definition of the coordinate axis shown in Fig. 4.4, and calling θ the angle between \mathbf{n} and the x-axis, we then have for the free energy in the one constant approximation,

$$F = 1/2 \int dV \left\{ K \left[\left(\frac{\partial \theta}{\partial x} \right)^2 + \left(\frac{\partial \theta}{\partial y} \right)^2 \right] - \frac{\epsilon_a}{4\pi} E^2 \sin^2 \theta \right\}. \quad (4.10)$$

The fundamental length scale, ξ , set by competition between elastic and electric forces is $\xi = (4\pi K/\epsilon_a E^2)^{1/2}$. From this, we get $\xi/2h = 0.22/V_v$ in 5CB, so that for V_v larger than a few volts, the free energy density is nonzero only in a region thin compared to the sample thickness. For distances much larger than ξ to the left of the defect, $(\partial\theta/\partial x)^2$ is negligible and since $\theta = \pi/2$ in the undistorted state to the right of the line, the region to the left has for $\ell \gg \xi$ an excess free energy per unit line length.

$$F_{\text{exc}} = \ell \int_{-h}^{+h} dy \left[\frac{K}{2} \left(\frac{\partial \theta}{\partial y} \right)^2 - \frac{\epsilon_a}{8\pi} E^2 (\sin^2 \theta - 1) \right] + F_{\text{core}}. \quad (4.11)$$

Here ℓ is the distance between the wire and the defect line and F_{core} is the free energy of the core region within a distance ξ from the line defect. To evaluate the first term in F_{exc} , we first express $(\partial\theta/\partial y)$ in terms of $\sin^2\theta$. The equation away from the disclination is

$$K \frac{\partial^2 \theta}{\partial y^2} = -\frac{d}{d\theta} \frac{\varepsilon_a E^2}{8\pi} \sin^2 \theta . \quad (4.12)$$

This is the equation for the conserved motion of a particle in a potential. Constancy of energy shows that

$$\frac{1}{2} K \left(\frac{\partial \theta}{\partial y} \right)^2 + \frac{\varepsilon_a}{8\pi} E^2 \sin^2 \theta = \text{const} . \quad (4.13)$$

On the boundaries, $\theta = \pm\pi/2$ and $(\partial\theta/\partial y)$ is negligible for $h \gg \xi$, hence, constant = $\varepsilon_a E^2/8\pi$. Eq. 4.13 then finally yields for F_{exc} .

$$F_{\text{exc}} = F_{\text{core}} + 2\ell \int_{-h}^{+h} dy \frac{\varepsilon_a}{8\pi} E^2 \cos^2 \theta = F_{\text{core}} + \ell \left(\frac{\varepsilon_a K}{\pi} \right)^{1/2} E , \quad (4.14)$$

where the integral was evaluated with θ as integration variable, using $dx = \xi d\theta / |\cos\theta|$.

The driving force for this motion is $-dF_{\text{exc}}/d\ell$ and we therefore expect on dimensional grounds an equation for the defect motion of the form

$$2b\gamma_{\text{eff}} \frac{d\ell}{dt} = -\frac{dF_{\text{exc}}}{d\ell} = -E \left(\frac{\varepsilon_a K}{\pi} \right)^{1/2} , \quad (4.15)$$

implying that the velocity [4.23] $c = -d\ell/dt$ is given by

$$c = \frac{E}{2b\gamma_{\text{eff}}} \left(\frac{\varepsilon_a K}{\pi} \right)^{1/2} . \quad (4.16)$$

In Eq. 4.15, γ_{eff} is an effective viscosity and b a dimensionless number of order unity. The term on the left hand side represents the friction that occurs in a region of size ξ near the defect where the director changes rapidly in time. The number b depends only on the details of the energy dissipation in this region, where the strain is singular. As a result, b will depend on the core size and may show some weak field dependence as well. A rough estimate (expected to be an overestimate²⁴) for b , obtained by approximating the structure near the defect by that of the defect in the absence of fields, gives $b \approx 2.1$ for fields strengths used in the experiments. Because the strain near the defect consists of both splay and bend, we take $\gamma_{\text{eff}} = 1/2(\gamma_{\text{bend}} + \gamma_{\text{splay}})$ where²⁵ $\gamma_{\text{splay}} \sim \gamma_1$, the orientation viscosity but, $\gamma_{\text{bend}} = \gamma_1 - \alpha_2^2 / (\eta_b - \gamma_2)$ because of back-flow effects. As mentioned earlier, the terms γ_{eff} and b on the left hand side of Eq. (4.15) both depend on the precise structure near the core, such as the splay/bend character of the strain and the core size. Since such details are not known with great accuracy, the above estimates are crude, and the approximation for γ_{eff} should be considered correct to only about 20%.

The data of Fig. 4.6(a) give $\beta = c/V_v = 4.7\mu\text{m/volt-sec}$, with an error of about 5% estimated from the scatter in the data. For 5CB at 30°C,²⁵ $\gamma_1 = 0.50\text{P}$, $(K_1 + K_3) / 2 = 5.5 \times 10^{-7}$ dyn, $\epsilon_a = 9.8$, $\eta_b = 0.25\text{P}$ and $\gamma_2 = -0.56\text{P}$. With these values, Eq. (4.16) predicts $\beta = c/V \approx 4.2 b^{-1}\mu\text{m/volt-sec}$. Comparison with the experimentally obtained value then gives $b \approx 0.9$, slightly more than a factor two smaller than the crude estimate. Fig. 4.6(b) compares the experimentally observed temperature dependence of β with the temperature dependence as predicted with the aid of Eq. 4.16 with fixed b . In both cases, the temperature dependence appears to be qualitatively correct.

While the data is interpreted as support for the basic notion that the director pattern simply translates in the applied field with a speed determined by balancing the viscous force against the elastic and electrostatic forces, a more stringent comparison of theory and experiment requires a closer examination of backflow effects (taken into account here in an approximate way by picking an effective viscosity that is the average of the pure splay and bend viscosities²⁶) and of the dissipation near the core. In this experiment, the driving force of the motion is accurately known (even when the splay and bend elastic constants are not the same²⁷ whereas the dissipation is determined only by details of the core structure, thus, this type of an experiment may well provide a way to study small scale properties of defects through their dynamics.²⁸

Although this experiment differs from most studies of defect dynamics in the precise control of the driving force (the combination of elastic and electrostatic energy), the picture obviously applies much more generally, as first realized by Dreizin and Dykhne^{29,30}. Usually, in less well controlled experiments, the excess free energy F_{exc} in Eq. (4.15) is not known accurately, but the order of magnitude and the dependence on the distance ℓ between defects or between the cell wall and a defect can be estimated. If so, the basic time dependence for the motion immediately follows from Eq. (4.15). Indeed, because of the logarithmic decay of the strain field associated with a free line defect, $F_{\text{exc}} \sim \ln \ell$ for two defect lines and so ℓ should vary as $\ell \sim (t_0 - t)^{1/2}$. A similar scaling can be developed for the collapse of circular domain walls.³¹ In this latter case, both F_{exc} and the dissipation are clearly proportional to the radius, R , of the domain, i.e.

$$\gamma_1 R(dR/dt) \sim dF_{\text{exc}}/dR = \text{const}, \text{ and hence, } R \sim (t_0 - t)^{1/2}.$$

4.3.2 Moving Wall Fronts in Helielectric Liquid Crystals

Many liquid crystal compounds are chiral: one or more carbon atoms bonds to four different groups making chiral molecules distinguishable from their mirror images. In the more fluid liquid crystal phases, they spontaneously form a macroscopic twisted structure with a pitch typically a few thousand angstroms to several microns. The smectic C phase formed by chiral molecules is called smectic C*. Similar to smectic A, there is layering on a microscopic scale and fluidity in the plane of the layers but the direction of orientational order is at an angle $\theta \neq 0$ to the layer normal and rotates in a helical fashion about it. Because of the local ordering of chiral molecules, the mirror symmetry is broken on scales much smaller than

the scale of the pitch. As a result, a spontaneous polarization can appear perpendicular to the component of \mathbf{n} in the plane of the layers. In the ground state, as \mathbf{n} rotates from layer to layer, the polarization, \mathbf{P} , also rotates about the layer normal so that, macroscopically, $\langle \mathbf{P} \rangle = 0$. These materials are called ferroelectric in the liquid crystal literature because of the existence of a local polarization. A suggestion³² has been made that *helielectric* is a more appropriate name for two reasons:

- i. It more accurately expresses the physics we may learn by studying bulk properties of this unique structure that has no analogue in solid-state physics;
- ii. The more crystalline phases of chiral molecules do not support a helical structure and these are indeed found to be ferroelectric in the usual sense.^{33,34}

However, when the helix structure is destroyed by surface forces, the sample exhibits some ferroelectric properties. This can be achieved with a thin cell, composed of two transparent conducting electrodes sandwiching a thin ($\sim 1\mu\text{m}$) layer of helielectric material with the twist axis in the plane of the electrodes. This sample configuration has been termed *Surface Stabilized Ferroelectric Liquid Crystals* or SSFLC by its inventors.³⁵

An interesting question is what happens to the helicoidal structure when a field is applied perpendicular to the helix axis of a bulk material in the helielectric state. Early studies³⁶ suggested that the helix could be completely unwound by a field applied in the plane of the layers much like the unwinding of the helicoidal structure of a cholesteric liquid crystal that does not have a microscopic layered structure so can unwind by, for example, escaping into the third dimension.⁵ Later, it was proposed³² that perhaps this was not the case because of the underlying layer structure that did not allow the director to escape in a similar way because the resulting change in the tilt angle, θ , would, in smectic C*, be associated with an energetically costly change in the layer spacing ($\sim 30\text{\AA}$).

The evidence presented for this point of view³² was the reversibility of the textures, described below, that are observed in smectic C* when the field is cycled from $E = 0$ to some finite value and then back to $E = 0$. This is not observed in cholesteric liquid crystals when the similar experiment is made.³⁷ In studying how the helicoidal structure returns in a material in the cholesteric phase that has been unwound by an electric or magnetic field, one observes that the process is non-trivial involving the nucleation and growth on a macroscopic scale of many defects. The texture is not reversible with field.

In smectic C*, on the other hand, the effect of an electric field must be different. If the polarization rotates about the z-axis, say, and the field is applied in the x-direction, then, at an arbitrarily small field, the only possibility consistent with the locking from the layer spacing is that those parts of the helix where is locally parallel to \mathbf{E} expand. Because of the periodicity of \mathbf{P} , this means that the "bad" regions where \mathbf{P} is anti-parallel to \mathbf{E} shrink. In this scenario, the high field picture is that of a periodic array of walls with a spacing given by the pitch. If the field is suddenly reversed, the "bad" regions become the "good" regions and a solitary wave propagates as the new stable regions grow at the expense of the new unstable ones. This

accounts for the absence of a coercive field for reversing the polarization: the cell starts switching as soon as the field is turned on. Fig. 4.7 is a sketch of this scenario.

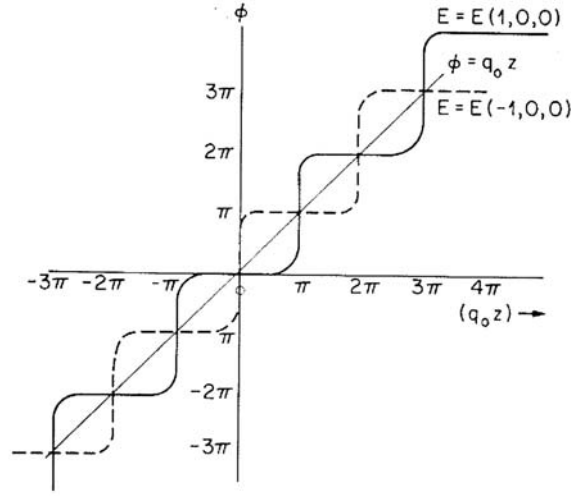


Fig. 4.7. ϕ as a function of $q_0 z$ for positive and negative fields.

To see this case, we assume all elastic constants equal, define a 2 dimensional director in the plane of the layers, $\mathbf{b} \neq -\mathbf{b}$, $\mathbf{b} = \mathbf{P}/P$ where $\mathbf{b} = (\cos\phi(z), \sin\phi(z), 0)$ and $\mathbf{P} = P\theta (-\sin\phi(z), \cos\phi(z), 0)$. If $\mathbf{E} = E(0, 1, 0)$, the free energy of this phase in an applied electric field, can be written as:

$$F = \int_z dz \left[\frac{K\theta^2}{2} \left(\frac{d\phi}{dz} + q_0 \right)^2 - \frac{\epsilon_a \theta^2}{8\pi} E^2 \sin^2 \phi - P\theta E \cos \phi \right]. \quad (4.17)$$

We adopt the usual convention that in a right hand coordinate system, $q_0 > 0$ is a right-handed helix. Minimizing Eq. (4.17) and equating it to the viscous damping $\gamma\theta^2 \mathbf{b} \times \dot{\mathbf{b}}$, leads to the Euler-Lagrange equation

$$K\theta^2 \frac{\partial^2 \phi}{\partial z^2} + \frac{\theta^2 \epsilon_a}{4\pi} E^2 \cos \phi \sin \phi - \theta P E \sin \phi = \gamma\theta^2 \frac{\partial \phi}{\partial t}. \quad (4.18)$$

To deduce the time dependence of the change in \mathbf{P} with change in sign of \mathbf{E} , it is usual to neglect the dielectric term, $\theta^2 \epsilon_a / 4\pi E^2$. To simplify the discussion, we, too, will do so initially and consider instead of Eq. (4.18)

$$\gamma\theta^2 \frac{\partial \phi}{\partial t} = K\theta^2 \frac{\partial^2 \phi}{\partial z^2} - EP\theta \sin \phi. \quad (4.19)$$

At the end of this section, we return to complications associated with the dielectric term.

Consider first the static case. In the absence of a field, the obvious minimal energy solution is the one with a uniform twist, $\phi = q_0 z$. For $E > 0$, the director twist is non-uniform. In particular, when the electric coherence length $\xi_E \equiv (K\theta/PE)^{1/2}$ is much smaller than the pitch, the relevant static states, according to the above picture, consist of domains of size equal to about the pitch with \mathbf{P} mostly parallel to \mathbf{E} . The domains are separated by walls of thickness ξ_E where the director rotates by about 2π , sketched in Fig. 4.7, where the profile $\phi(q_0 z)$ consists of an array of walls separating regions where $\phi \approx 2\pi$ (for $E > 0$) or $\phi \approx 2\pi(k + 1/2)$ (for $E < 0$) and k is an integer. Clearly, when the field direction is reversed, the large domains become unstable because \mathbf{P} and \mathbf{E} are antiparallel. As a result, we then expect each wall to split into two kinks or domain walls propagating in opposite directions into the neighboring unstable states. Hence this experiment constitutes an example of the type of front propagation into an unstable state amenable to a marginal stability analysis, as mentioned in the introduction to section 4.3.

Since the thickness of the wall is much less than the pitch $2\pi/q_0$, we expect that over most of the distance each wall propagates, its speed will be close to some asymptotic speed, c , that on dimensional grounds must be of order ξ_E/τ_E , where $\tau_E = \gamma\theta/EP$. This suggests analyzing uniformly translating wall solutions of the form $\phi(z - ct)$. In dimensionless coordinates (in units of ξ_E and τ_E) these profiles satisfy for $E > 0$

$$\frac{d^2\phi}{du^2} = \sin\phi - c\frac{d\phi}{du}, \quad (4.20)$$

where $u \equiv z - ct$. As in the case of the Freedericksz transition, this equation is the same as the one determining traveling wave solutions of the sine-Gordon equation with damping.

Eq. (4.20) illustrates an important feature commonly found for front propagation into an unstable state: the asymptotic velocity, c , can not be determined solely from an analysis of the uniformly traveling wave solutions.³⁸ To see this, note that Eq. (4.20) is equivalent to the equation of motion for a particle subject to friction moving in a potential $V = c\cos\phi$. In this analogy, u plays the role of time and c the role of a friction constant. Let us consider the case where the field has just been flipped to a positive value and a front is propagating into the unstable state, $\phi = \pi$. This potential is illustrated in Fig. 4.8a and 4.8b by the case $\Delta < 1$ (we define Δ in Eq. 4.16 but to illustrate the physics of this part of the problem the definition of Δ is not needed). In the analogy with the ‘particle in a potential’, the unstable state corresponds to $\phi = -\pi, 3\pi, \dots$ and the stable state to $\phi = 0, 2\pi, \dots$. The solution we are interested in is the one where the ‘particle’ starts at the top of the potential ($\phi = \pi$, say) at ‘time’ $u > -\infty$ and comes to rest in the bottom of the potential ($\phi = 0$, say) for long times ($u \rightarrow \infty$). Clearly, physical insight tells us that a solution exists for any value of the ‘friction constant’, c . In other words, the front propagation speed, c , cannot be determined by steady state considerations alone, and apparently the value of the velocity is ‘selected’ by some kind of a dynamical mechanism.

This velocity selection mechanism is actually well understood mathematically³⁸ as well as physically:¹⁷ the asymptotic speed at which most fronts (*i.e.* those where $\phi(z, t = 0)$ is different

from the unstable value in a sufficiently localized region) propagate, is the slowest one to maintain a stable moving profile and corresponds to the so-called marginal stability point that can be explicitly calculated.¹⁷ For Eq. 4.13, this speed is 2 and translates in dimensional units to:

$$c = 2\xi_E/\tau_E = \frac{2}{\gamma} \left(\frac{EPK}{\theta} \right)^{1/2} . \quad (4.21)$$

The square root field dependence of the speed was previously predicted to occur on dimensional grounds.³² Although this expression is reasonably consistent with the values of the front speed inferred from the experiment, it should be kept in mind that we have so far only considered the long time (asymptotic) front speed, c , predicted by marginal stability. For moderate fields so that ξ_E is much smaller than the pitch, initial transients will have to be taken into account.³⁹

Let us now briefly comment on the case where the dielectric term $\epsilon_a E^2$ is not negligible, so that the free energy density associated with the field interaction is

$$F = -\frac{\theta^2 \epsilon_a}{8\pi} E^2 \sin^2 \phi - PE\theta \cos \phi . \quad (4.22)$$

While the polarization term is sensitive to a sign reversal of the electric field, the dielectric term is not. Consequently, when the field is strong enough so that the first term dominates, inverting the field direction does not necessarily bring each domain into an unstable state. To discuss this in more detail, we analyze the behavior of F as a function of the angle ϕ and the ratio

$$\Delta = \frac{|\epsilon_a E| \theta}{4\pi P} \quad (4.23)$$

that measures the relative importance of the dielectric term. Note that F remains unchanged when we simultaneously reverse the sign of E and increase ϕ by π . Thus we draw F for positive E only, keeping in mind that the effect of a sudden reversal of the field on a domain in the lowest energy state ϕ_0 is equivalent to putting the domain in the state $\phi_0 \pm \pi$.

As shown in Fig. 4.8(a) and (b) for both signs of ϵ_a , we can distinguish four different cases:

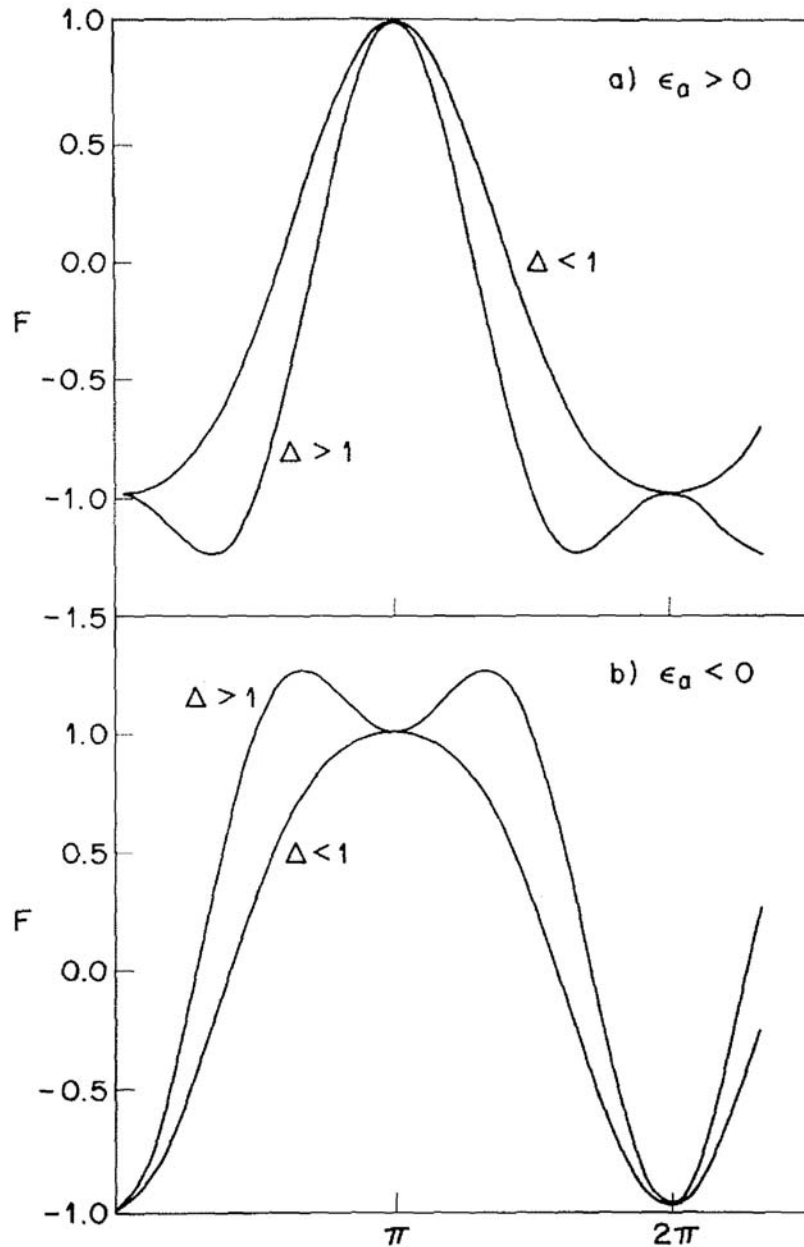


Fig. 4.8. The potential, F [Eq. (4.22)] for (a) $\epsilon_a > 0$ and (b) $\epsilon_a < 0$.

- i. When $\Delta < 1$ (small fields), a reversal of the field brings the domains into an unstable state for positive as well as negative ϵ_a , so that we may expect the front velocity to be given by a marginal stability type expression such as Eq. 4.21.
- ii. As $\Delta \rightarrow 1$, the effect on the potential is different for the two signs of ϵ_a . For $\epsilon_a > 0$, the dielectric energy increases the front velocity, as it increases the maximum of the potential at $\phi = \pi$ relative to the minimum at $\phi = 2\pi$. For $\epsilon_a < 0$, increasing Δ flattens the

maximum (so that it becomes a local minimum when $\Delta \rightarrow 1$), and this tends to decrease the velocity. In such a case, the straight forward marginal stability expression ("case I" of Ben-Jacob et al.¹⁷) predicts a maximum velocity when $\Delta = 1/2$ and a speed of zero when $\Delta = -1$. As we discuss, in the next section, in the regime, $1/2 < \Delta < 1$, we may find case II marginal stability when $\varepsilon_a < 0$ ¹⁷.

- iii. When $\Delta > 1$ and $\varepsilon_a < 0$, a reversal of the field brings stable domains into a metastable state, and the resulting wall propagation will be qualitatively and quantitatively different from case (i). This case is also discussed in the next section.
- iv. For $\Delta > 1$ and $\varepsilon_a > 0$, the minimum energy state shifts away from 2π to ϕ_0 , say. Therefore, a reversal of the field, equivalent to $\phi_0 \rightarrow \phi_0 \pm \pi$, lands the system off the potential maximum. This, then, is equivalent to preparing the domains in an unstable state with a finite driving force (since $dF/d\phi \neq 0$), and one expects a homogeneous relaxation of domains. We do not discuss this case at all.

Clearly, the present system may provide a unique opportunity to study the various forms of front propagation and the cross-over between these regimes. In the next section, we analyze some features that emerge when the case $\varepsilon_a < 0$ is considered within the context of the above discussion.

4.3.3 An Exact Solitary Wave Solution for ε_a

Here we discuss an exact solution that exists for $\varepsilon_a < 0$.⁴⁰ The regime $\varepsilon_a > 0$ has also been considered from a different perspective by Coleman⁴¹ and his analysis may be illuminating for understanding some of the fascinating electro-hydrodynamic instabilities that are sometimes observed in this phase.

As we shall see, an exact solution is of practical interest in the light of the previous discussion. Furthermore, the solution may also be of interest from a nonlinear dynamics perspective as well: it can serve as a starting point for a perturbation expansion to study the effect of additional terms.⁴² Finally, it may be used as a further test of the connection between the Painlevé property (the existence of movable poles in the complex plane) and the integrability of a nonlinear equation.⁴³

In terms of the dimensionless coordinates used before, Eq. 4.11 for $\varepsilon_a < 0$ becomes

$$\frac{d^2\phi}{du^2} - \Delta \sin\phi \cos\phi = \sin\phi - c \frac{d\phi}{du}, \quad (4.24)$$

with Δ given by Eq. (4.16). It is easy to check that when we solve the equation by equating the right hand side to zero, the left hand side equates to zero too,⁴⁴ provided $\Delta = c^2$. The exact solitary wave solution is: $\tan\phi/2 = \exp[z / \xi_E \pm ct / \tau_E]$, with $c = \Delta^{-1/2} \xi_E / \tau_E = (2P/\theta\gamma)(\pi K/\varepsilon_a)^{1/2}$ and is *independent* of the applied field.

Physically, unlike the marginal stability strategy where the velocity is determined by a competition between a driving term and elastic terms defining the front profile, here, a speed is selected to balance exactly the driving term leaving the front profile to be determined by a balance between the elastic and dielectric terms. Interestingly, this solution makes no demands on the relative magnitude of the dielectric and the polarization terms. However, physically, owing to the periodic nature of helielectric phases, the field must be large enough to accommodate the width of a single solitary wave within a half pitch, making reliable data impossible to obtain at small fields.

In the regime, $\Delta < 1/2$, the more relevant solution is not the exact solution but the dimensionless marginal stability solution with a speed $c = 2(1 - \Delta)^{1/2}$. Thus, when $\Delta = 1/2$, the speed (and its first derivative with respect to E) given by the exact solution coincides with the speed predicted by marginal stability. A preliminary analysis⁴⁰ similar to the one performed by Ben-Jacob et al.¹⁷ for $1/2 < \Delta < \sim 1$ shows that it corresponds to the regime they call "case II marginal stability". In this regime, front profiles with speed slower than $\Delta^{-1/2}$ are unstable to "a localized mode", and therefore, they argue, the relevant front profile is the one for which we found the exact solution with $c = \Delta^{-1/2}$.

Finally, when $\Delta > 1$, the earlier analysis shows that the present solution describes front propagation from a *metastable* state into a stable state, and since this solution can be shown to be unique, the exact solitary wave solution must be the relevant one. If experiments could be done in this regime, one should then see a front velocity independent of the field strength!

Including the inertial term leads to a relativistic-like form for the front speed of the exact solution so, we may speculate as Kamenskii⁹ did, that precise experiments performed in these systems may also lead to an understanding of the role this term plays in these materials.

4.3.4 Biological Significance of Chirality

It is well-known that chiral-molecules form the building blocks of biological systems. It is, perhaps, less well-known that parts of the brain and cell membranes are actually in the liquid crystal state. For example, the lipid molecules that form the 2-d cell membranes are chiral and in a liquid crystal state (probably smectic C*) so that many functions vital to the living process depend on the collective dynamic and equilibrium properties particular to mesophases (as opposed to crystal order). An example of this is the propagation of electric signals through nerve sheathes that, as mentioned earlier, is closely related to the motion of walls in liquid crystals. Xin-yi¹⁸ has modeled this problem using front propagation in nematics. Here we point out that possibly, smectic C* may provide additional insight into this problem since it is chiral and its spatial symmetry is more closely related to biological systems.

Another amusing liquid crystal example, perhaps applicable to biological problems, is found when observing two $S = -1/2$ line defects in a capillary filled with material in the cholesteric liquid crystal phase. At a temperature close to the transition temperature to the smectic A phase,⁵ the elastic constants are stiff so the two line defects remain parallel to each

other and try to maximize the distance separating them. Upon slight heating to soften some of the elastic constants, the lines wind up as a regular double helix with handedness opposite to the chirality of the material. Although the scales are different, studying the dynamics of this process may well provide another dimension to our understanding of the similar process that occurs in chiral polymers of living systems like DNA.

4.3.5 Nonlinear Aspects of Liquid Crystals in Flow

The simplest properly invariant theory to describe the director response to velocity gradients was first given by Ericksen.⁴⁵ His theory was specialized to the case of nematic liquid crystals by Leslie.⁴⁶ Ericksen⁴⁵ shows that in simple shear, $v_1(x_3)$, say, there is a torque acting on \mathbf{n} to align it in a fixed direction given by $\tan^2\theta = \alpha_3/\alpha_2$. θ is the angle between \mathbf{n} and the velocity, \mathbf{v} . α_3 and α_2 are two of the six Leslie viscosities, α_i ^{26,46} that reduce to five linearly independent ones, when Parodi's relation⁴⁷ is assumed. When $\alpha_3/\alpha_2 \rightarrow 0$, there are actually four solutions to this equation: $\pm\theta$ and $(\pm\theta + \pi)$. Two of the solutions are stable and two are unstable. When the stable solutions apply, the effect is known as *flow alignment*.

Evidently, the existence of θ depends crucially on α_3 and α_2 having the same sign (usually both negative). It may not be true for some nematics. When α_3 and α_2 are of different signs, a spatially constant, stationary value for θ cannot be defined. Rather, θ , and hence the elastic energy, increases continuously in time, eventually leading to a dense formation of defects - orientational turbulence.

In liquid crystals that exhibit both nematic and smectic A phases, α_3 depends strongly on temperature going from a negative value far from the transition temperature to a large positive value just before the transition to the smectic A phase. However, the magnitude and sign of α_2 are unaffected by smectic A fluctuations. In our third example, we show how this feature makes nematic phases of these compounds the ideal arena to study the interplay between elastic and viscous torques for a large range of values of material constants. As we shall see, this example differs from the previous ones in that it has so far, not been analyzed quantitatively. As it illustrates several dramatic consequences of the coupling between flow and director motion, it may, however, be a fruitful subject for further study.

A Scenario for Director Turbulence

The sample geometry is the Couette geometry: a fixed outer cylinder with a concentric inner cylinder that rotates about the z-axis.^{48, 49} The liquid crystal material resides in the space between the two cylinders and does not exhibit flow alignment. Small glass tubes (~1mm i.d.) and glass shafts (~0.5mm o.d.) are treated so that the boundary conditions for \mathbf{n} is radial on the glass surfaces. This is the same boundary conditions as the one that was imposed on the capillaries discussed in section 4.2.2. In this case, the inner shaft acts as a large core region so the director does not escape into the third dimension when the inner shaft is at rest: it remains in the (r, ϕ) plane.

Once the liquid crystal is sheared, however, a sequence of stationary states are observed for the director that, with increasing shear, results in the sample becoming optically opaque as a dense spool of disclination threads nucleates on and winds up around the inner shaft to fill the gap of the cylinder. We now propose to describe the sequence of instabilities that occur with increasing shear as the system makes transitions from one stationary state to another and that end in what we call, loosely speaking, director turbulence. In this regime, the simple strategy of balancing elastic and viscous torques is no longer useful.

At rest, the director has only a radial component, n_r . Once the inner cylinder is set into motion it develops an azimuthal component, n_ϕ , that reaches a maximum somewhere between the two cylinders then decreases to zero on the cylinder walls. At low shears, the director remains in the plane of shear, the (r, ϕ) plane. With increasing shear, the maximum value of n_ϕ increases, since there is no flow alignment and elastic forces are weak. Once it exceeds $\pi/2$, a first tumbling instability is observed when the elastic and viscous torques now act in cooperation to create a solitary wave instability involving a propagating change in the director orientation. It can be proven optically that the director orientation is only in the (r, ϕ) plane during and after this instability.^{48,49}

Once the director escapes the plane of shear, a cellular instability is triggered (Fig. 4.9) that is similar but distinct from Taylor cells.¹⁰ An important observation made here was that when $\gamma_2 = \alpha_3 + \alpha_2 = 0$, the viscosity coefficient controlling director response to irrotational shear, \mathbf{n} cannot escape the plane of shear: the cellular instability is *not* observed and director turbulence *does not* take place. Indeed, we learned that perfectly oriented cells could be rapidly manufactured after filling by setting the temperature to the value where $\gamma_2 \sim 0$ and rotating the inner shaft at several thousand rpm's for a second or two. This process was much faster than waiting the several minutes it takes for feeble elastic forces to establish boundary conditions. However, at any temperature other than the one corresponding to $\gamma_2 \sim 0$, this procedure results in a highly disordered cell, as we shall see.

The interesting feature of the cells is the change in their cross-section in the (r, z) plane with increasing shear. At low shear, the cross-section is nearly square. With increasing shear, it becomes more rectangular by remaining constant in the r direction and shrinking in the z direction: the wavelength of the cells decreases with increasing shear. When it becomes so small that mechanical instabilities associated with the rotation of the inner shaft, perhaps, or other fluctuations in other external parameters cause them to overlap, disclination threads nucleate and grow around the inner shaft. Eventually the threads completely fill the gap and observations are no longer possible. The observations ended in "director turbulence".

The interesting feature of the cells is the change in their cross-section in the (r, z) plane with increasing shear. At low shear, the cross-section is nearly square. With increasing shear, it becomes more rectangular by remaining constant in the r direction and shrinking in the z direction: the wavelength of the cells decreases with increasing shear. When it becomes so small that mechanical instabilities associated with the rotation of the inner shaft, perhaps, or other fluctuations in other external parameters cause them to overlap, disclination threads

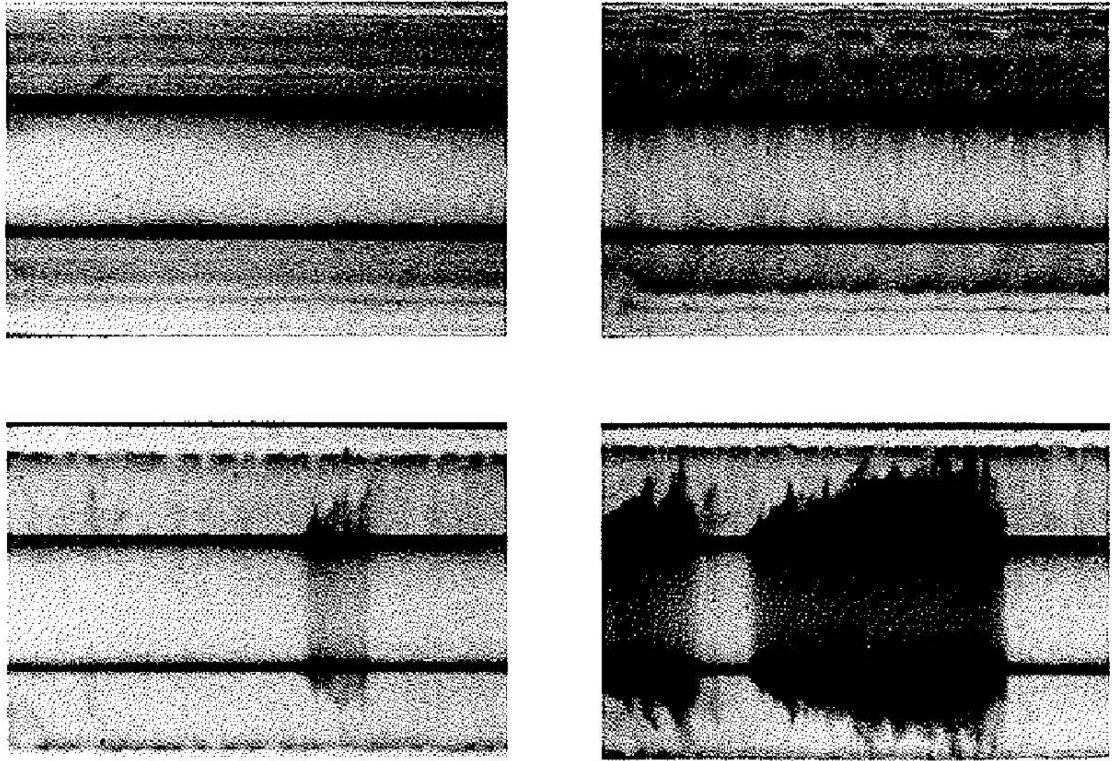


Fig. 4.9. Photomicrographs, polarizers crossed 45 degrees to the frames, of Couette flow in a liquid crystal for which $\alpha_1 / \alpha_2 < 0$ (CBOOA). Top right is the cellular flow regime. Bottom left shows disclinations nucleating on the inner shaft as the cells become more compressed. Bottom right shows the continuations of bottom left. The observations ended when the cell became opaque from the large density of disclination lines (Ref. 49).

nucleate and grow around the inner shaft. Eventually the threads completely fill the gap and observations are no longer possible. The observations ended in "director turbulence".

In a larger Couette cell (2cm i.d. outer cylinder and 1cm o.d. inner cylinder) and a liquid crystal that supports flow alignment, it was unusual to start from rest with a well-oriented cell. Masses of disclinations are observed floating in the gap during shear. However, once the Taylor instability sets-in, a regular pattern is set up where disclinations are organized in clumps within each cell. This made an amusing pattern that effectively visualized each of the Taylor cells (Fig. 4.10).

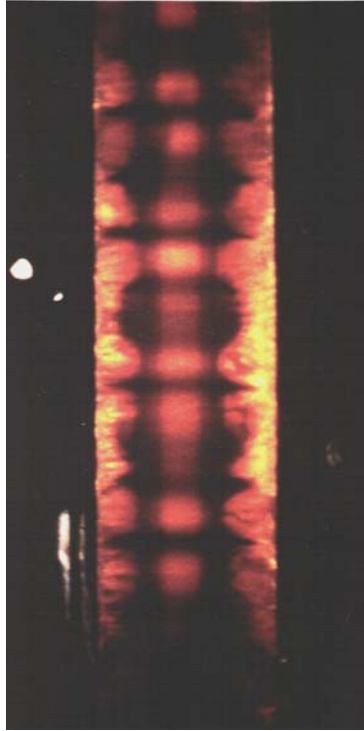


Fig. 4.10. Disclination lines decorating the Taylor cells in a nematic liquid crystal [Ref. 49].

Thus, to reduce complications in a study of nonlinear dynamics of anisotropic liquids, it is useful to find a system, or geometry, where the orientation of the director relative to the plane of shear can be controlled. This was found by going to smectic C films that we describe in the next example.

Phase Winding and Flow Alignment in Freely Suspended Films of Smectic C Liquid Crystals

A density wave in one direction and orientational order in another, characterize smectic C liquid crystals. In general, the hydrodynamic equations for smectic C^{50, 51} are complicated making flow studies impractical when both density wave and orientational order are involved. But, as discussed above, we want to take advantage here of the simplifying features of the anisotropic 2-d flow behavior that is expected for shear applied in the plane of a set of parallel layers.^{51,52}

Parallel layers are achieved by drawing freely suspended films across a circular hole and shear is applied by a rotating needle in the center of the film (Fig. 4.11).⁶ Depending on the topology of \mathbf{n} , we find two regimes. The first is the phase winding regime obtained when the film is free of defects so that the topological index, S , of the film is zero. Here, one observes concentric rings of constant angle, Φ , relative to the radial vector from the center of the cell. Φ assumes its maximum, Φ_0 , at the needle boundary layer, r_0 , and is zero at $r = R$, the film

radius. Φ_0 increases by 2π with each turn of the needle. Since the orientation is fixed at the rim of the film, rotating the needle winds \mathbf{n} up. The second regime is a flow alignment regime that occurs when the needle is at the center of a defect of topological index $S = +1$ where \mathbf{n} has circular symmetry. These results demonstrate the importance of topology in determining possible states for systems showing anisotropic behavior in 2-d.

The films studied had diameters $2R \sim 0.8$ to 2.6 mm and a thickness of $0.5 - 2\mu\text{m}$. They are drawn in an oven and observed with a polarizing microscope. Here, results obtained in the smectic C phase are discussed. The results for several materials showing this phase were all qualitatively similar. The quantitative data shown here were obtained using TB9A (terephthalylidene-bis (4 nonylaniline))⁵³ that exhibits the C phase between 157.5°C and 192.7°C as well as several other smectic phases.

We start the experiment from an initial state where Φ is a constant for $r_0 \leq r \leq R$. We insert the tip of a glass needle, $r_0 \approx 20\mu\text{m}$ into the film so that it is concentric with R . Rotation of a well-centered needle exerts circular shear on the film (Fig. 4.11). The angular speed of the needle can be as high as 5000 rpm.

In the phase winding regime, a $2\pi k$, k an integer, rotation of the needle results in a $2\pi k$ increase of Φ at r_0 relative to the phase at R . This is seen in polarized light as $4k$ dark concentric fringes (Fig. 4.12a and b with a schematic of the director orientation shown inset in Fig. 4.13a). The number of rings is determined by the number of rotations until a saturation is reached where the phase apparently slips at the needle boundary layer. This occurs when the radial width of the rings is comparable to the film thickness. Thinner films support more rings.

As long as the needle remains in the film, the picture of concentric rings does not change even if the needle stops rotating because the boundaries of the film pin Φ . Furthermore, reversing the rotation direction leads to an unwinding of the ring structure.

If the needle is pulled out of the film, the $S = 0$ topology is revealed as the needle area is replaced by uniformly oriented material. This is schematically shown as an inset in Fig. 4.13b. The phase at the center of the film unwinds in a characteristic time, τ , proportional to $K/\gamma_1 \approx 10^{-4}$ cm²/sec where K is elastic constant and γ_1 , a viscosity. This is observed as concentric fringes that shrink and vanish at the center of the film.

The flow alignment regime is seen in the polarizing microscope (Fig. 4.12c) as four dark brushes radiating from the needle. The topological index for this configuration is $S=+1$ since the orientation of \mathbf{n} changes by $1 \times 2\pi$ around any circuit that includes the needle. The needle forms the core of the disclination. Pulling out the needle creates a singular core at $r = 0$. As we will see, flow alignment cannot be obtained in circular shear without an $S = +1$ defect centered at the needle.

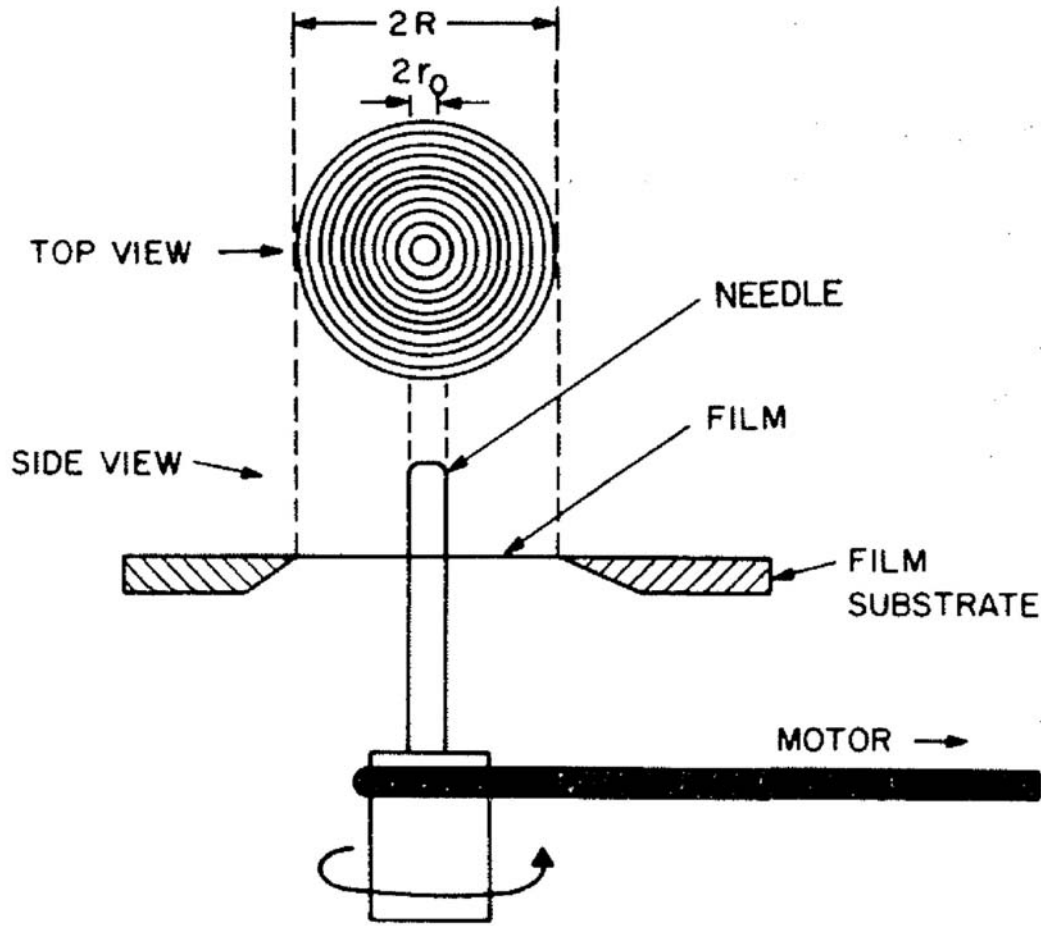


Fig. 4.11 Experimental set-up to observe freely suspended smectic C films in shear (Ref. 6).

To describe the phenomena observed, we note that the hydrodynamic equations for the in-plane director of smectic C^{51,52} specialized to the present geometry are isomorphic to those of a 2-d nematic and we can equivalently use the equations of Ericksen⁴⁵ specialized to two dimensions. We use polar coordinates (r, ϕ, z) and the in-plane director \mathbf{b} is given by $b_r = \cos\Phi$, $b_\phi = \sin\Phi$ but $\mathbf{b} \neq -\mathbf{b}$. A uniformly oriented film is thus described by $\Phi = \Phi_0 - \phi$ and an isolated disclination of index $S = +1$ by $\Phi = \text{constant}$. In general, for index S , $\Phi = (S - 1)\phi + \text{constant}$, where S is an integer.

In the geometry of these experiments, only two of the elastic constants for a smectic C liquid crystal are needed and they are assumed to be equal. The elastic energy, then, is:

$$F_{el} = \frac{K}{2} \int \left\{ [1 + (\partial\Phi/\partial\phi)]^2 + (r\partial\Phi/\partial r)^2 \right\} \frac{dr}{r} d\phi \quad (4.25)$$

when

$$\Phi = (S - 1)\phi + f(r) . \quad (4.26)$$

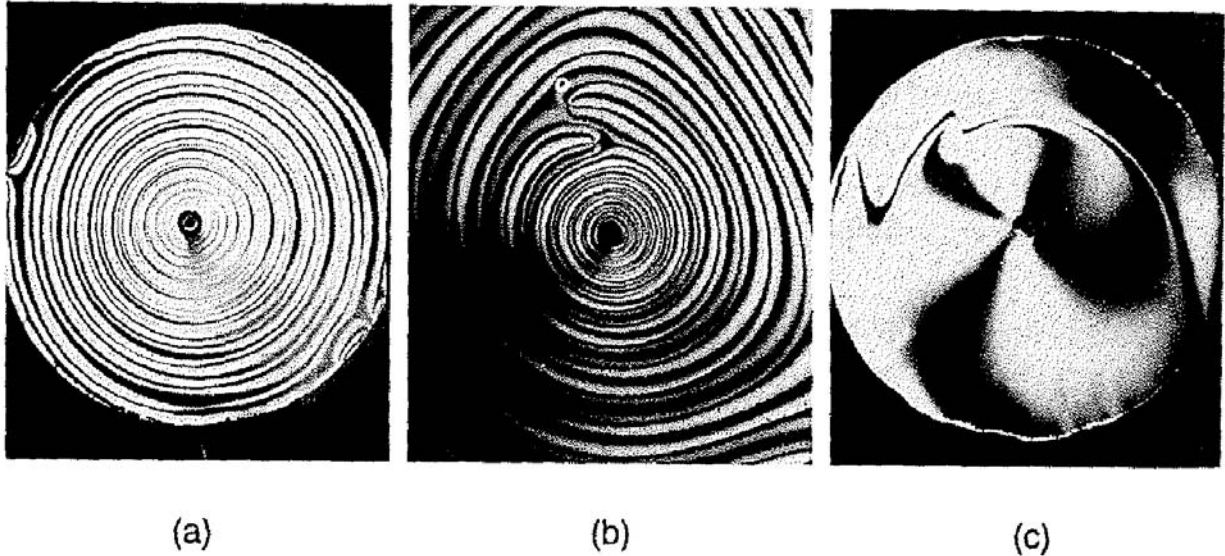


Fig. 4.12. Photomicrograph showing (a) phase winding, (b) disclination pairs that form when a ring breaks. They mediate the transition between the phase winding regime and the flow alignment regime shown in (c) Ref. 6.

Minimizing Eq. 4.25 with boundary conditions $\Phi = -\phi$ at $r = R$ and $\Phi = -\phi + \Phi_0$ at $r = r_0$, we obtain the static solution,

$$\Phi = -\phi + \Phi_0 \frac{\ln(r/R)}{\ln(r_0/R)} \quad (4.27)$$

predicting a logarithmic dependence of Φ on r when $S = 0$. In Fig. 4.13(a), we plot Φ versus r measured at constant ϕ by direct observation in the microscope. The agreement with Eq. 4.20 is clearly excellent. In the phase winding regime, Φ_0 is a function of time. For every 2π rotation of the needle, Φ_0 increases by 2π and the elastic energy stored in the film is, from Eqs. 4.25 and 4.26, $F_e = \pi K[\Phi_0^2 / \ln(R/r_0)]$.

To describe the relaxation of the rings when the needle is pulled out of the film, Eq. 4.25 is again minimized and a simple exponential decay is assumed for the time dependence of the director orientation. We obtain:

$$\frac{K}{r^2} \frac{\partial^2 \Phi}{\partial \phi^2} + \frac{K}{r} \frac{\partial}{\partial r} r \frac{\partial \Phi}{\partial r} = \gamma_1 \frac{\partial \Phi}{\partial t} \quad (4.28)$$

A time dependent solution of Eq. 4.21 that has the static result (Eq. 4. 20)) as an initial condition at small r , is

$$\Phi(r, \phi, t) = -\phi + \Phi_0 \frac{K_0(r/R)}{K_0(r_0/R)} \exp(-t/\tau) , \quad (4.29)$$

where K_0 is the modified Bessel function of the second kind⁵⁵ and $\tau = R^2\gamma_1/K$.

To check Eq. 4.29, we measured the time dependence of Φ at $r = 0$ with a video camera and a photo-diode. Fig. 4.13b shows Φ as a function of time for a typical run. The time constant, τ , is the inverse of the slope in Fig. 4.13b. Again quantitative agreement is found between predictions and observations. The R^2 dependence of τ can be verified by repeating the experiment for various film diameters. A plot of $\ln(\tau)$ versus $\ln(R)$ gives a slope of 1.9 ± 0.1 . A plot of τ versus R^2 gives $\gamma_1/K = 7.7 \times 10^3 \text{sec/cm}^2$, that is, about a hundred times smaller than in nematics ($\gamma_1/K \approx 5 \times 10^5 \text{sec/cm}^2$) and about the same as smectic C films only two or three layers thick⁵⁶ ($\gamma_1/K \approx 10^4 \text{sec/cm}^2$).

To describe the flow regimes, we assume that the velocity profile, $v_\phi(r) = r\omega(r)$, is given simply by the large gap approximation to the Navier-Stokes equation for circular shear⁵⁷, i.e. $v_\phi(r) \approx 1/r$. Then for fixed but arbitrary S , we obtain

$$K\gamma_1^{-1} \left(\frac{1}{r} \frac{\partial}{\partial r} r \frac{\partial \Phi}{\partial r} + \frac{1}{r^2} \frac{\partial^2 \Phi}{\partial \phi^2} \right) = \frac{\partial \Phi}{\partial t} + \frac{\omega_0 r_0^2}{r^2} \left(S - \lambda^{(3)} \cos 2\Phi \right) . \quad (4.30)$$

Given the initial dependence (Eq. 4.26) of Φ on the spatial coordinates, (r, ϕ) , Eq. 4.30 shows that only $S = 1$ has a stationary solution. Furthermore, for constant rotation, a given ring pattern such as the one shown in Fig. 4.12a, is stationary only when the phase slips at the needle boundary. On the other hand, for $S = 1$, a stationary flow alignment solution, Φ_A , is possible where $1/\cos 2\Phi_A = \lambda^{(3)}$ as predicted.⁵² From the form of this solution, clearly, flow alignment cannot occur in materials where $\lambda^{(3)} < 1$ even if $S = +1$.

Fig. 4.12c is a typical picture of flow alignment where the four black brushes crossing at the needle are the signature of the axial symmetry of an $S = +1$ disclination. Since these brushes are nearly at 45° to the direction of the crossed polarizer and analyzer, $\Phi_A \approx 45^\circ$ so that $\lambda^{(3)} \gg 1$. When the needle is in the film, it forms the core of the disclination. Pulling out the needle results in a singular core at $r = 0$. The static elastic energy (in the one constant approximation) for $S = 1$ with the needle in the film is just $F_\phi = \pi K \ln(R/r_0)$.

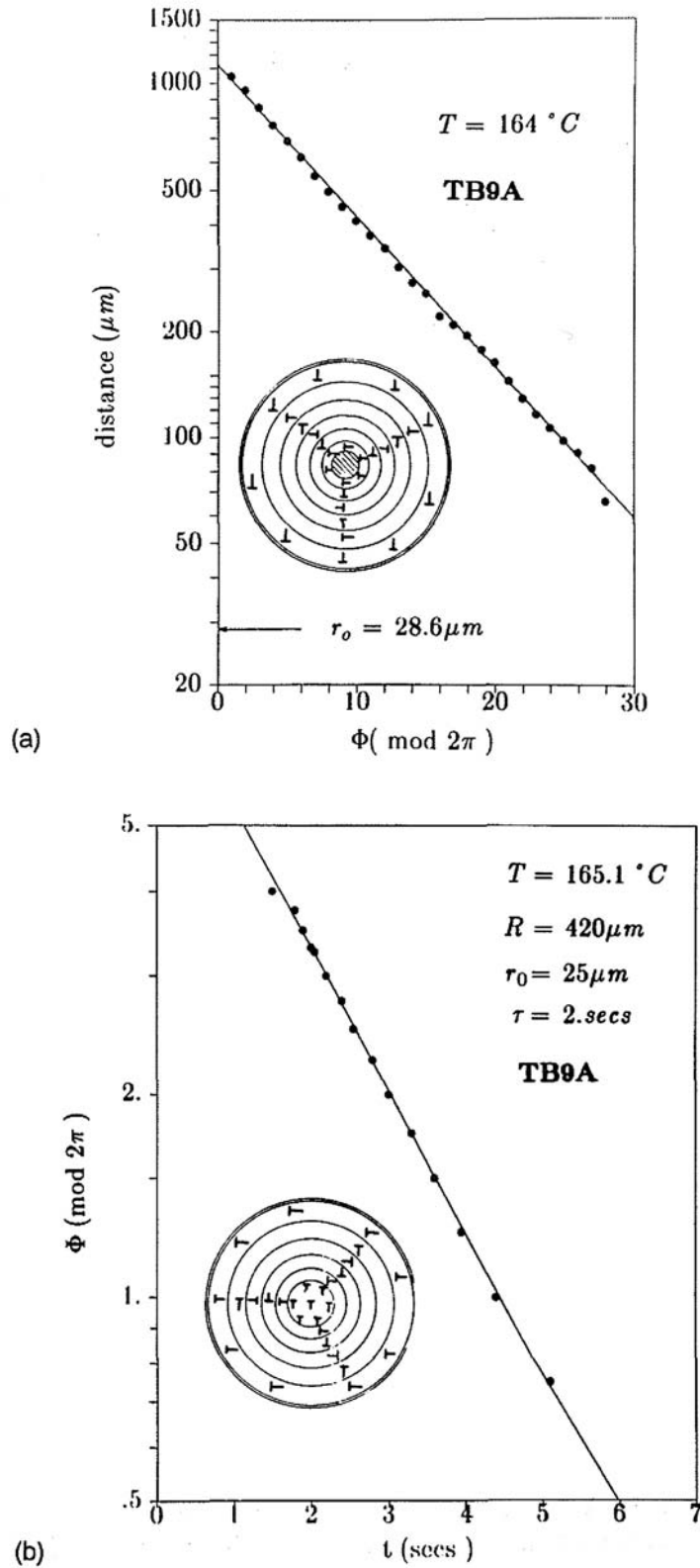


Fig. 4.13. (a) The ring position as a function of r , the distance from the center of the film. The ring structure is sketched in the inset. (b) $\mathcal{L}(\Phi)$ as a function of time during phase unwinding Ref. 6.

When $S = 0$, the coupling of \mathbf{n} to the rotational part of the shear cancels exactly with the convective term. The extensional part of the shear cannot now be balanced by the rotational part so Φ winds up (Fig. 4.12a). Such a scenario was first envisaged by de Gennes²⁶ when flow alignment was not an option for nematics because λ was smaller than 1. Although the elastic energy increases as the ring count goes up, there are no elastic counter-torques to stop the production of rings and a stationary state is only achieved when the phase slips at the needle boundary. It is possible that the slip condition is mediated by a thin region next to the needle transforming to the non-tilted smectic A phase.

In conclusion, two different flow regimes have been characterized in freely suspended smectic C liquid crystal films undergoing shear flow in 2-d:

- i. a flow alignment regime that had been previously predicted by Brand and Pleiner.⁵² In circular shear, a defect of strength, $S = +1$ centered around the needle is required to observe flow alignment and the flow alignment parameter was found to be large.
- ii. a phase winding regime that occurs when $S = 0$. In this regime, γ_1/K can be measured and was found to be $\approx 7.7 \times 10^3 \text{ sec/cm}^2$ for TB9A at $\approx 165^\circ\text{C}$.

Disclination pairs, forming when rings break, mediate the transition between these two states.⁶

4.4 1989 Perspectives with Some Up-dates Added 4/16/06

In this chapter we have focused on a few examples of experiments on liquid crystals that are of interest or their nonlinear or topological aspects. In fact, in the last few years, it has become clear in many fields of physics that liquid crystals offer unique opportunities to unravel important aspects of a large number of basic problems. We list here a few of these, without discussing them in any detail.

- i. Lowe and Gollub⁵⁸ have used liquid crystals to study the commensurate-incommensurate transition when a spatially periodic pattern is perturbed with an electric field with a different wavelength.
- ii. The measurements of Pindak et al.³¹ on the collapse of two-dimensional droplets in smectic C* films may provide a direct test of the Lifshitz-Allen-Cahn predictions for droplet dynamics.⁵⁹ If scattering experiments could also be performed on such films, it might yield a direct test of the non-conserved ordering dynamics in two dimensions.
- iii. Electrohydrodynamic instabilities are another interesting effect that illustrates changing spatial patterns with increasing voltage across a nematic liquid crystal. It is now possible to control the sample geometry so that cells with large aspect ratios can be studied under controlled conditions. For example, in a recent series of beautiful experiments, Steinberg and Rehberg⁶⁰ studied a traveling wave instability that they discovered in samples

thinner than 20 μm . They found that it was necessary to make cells whose thickness was precisely controlled over the whole cell. Failing this a reliable voltage threshold could not be determined. Furthermore, to study the patterns in terms of auto-correlation and cross-correlation functions, the temperature had to be controlled to within 1mK. They studied a large aspect ratio system of several hundred rolls that appeared with no imperfections. They found that the transition to the traveling wave state was second order. Above threshold, they observed that defects were created in the traveling wave patterns in greater number the further they were above threshold terminating, finally, in spatial turbulence.

Update: Cécile Fradin et al. Wavelength Doubling Cascade to Möbius Defect Turbulence in a 3D Anisotropic Liquid, [Phys. Rev. Lett. 81, 2902 \(1998\)](#) where a wavelength doubling cascade from a uniform state to a turbulent pattern is observed in a 3D anisotropic liquid (nematic). First oscillating convective rolls followed by a stationary stripe pattern, then Möbius defect creation stabilizing an unusual curved roll pattern that eventually becomes turbulent. Once created, Möbius defects are topologically trapped and the initial uniform state is not recovered. The system experimentally investigated is electroconvection above a highly nonlinear base state.

- iv. Recently, Oswald et al.⁶¹ have started a series of experiments on directional solidification in liquid crystals. The significance of these experiments is that they yield information on pattern formation near weakly first order transitions. For reasons discussed by Oswald et al.⁶¹ the results are qualitatively different from those found for materials with a strongly first order transition.
- v. Similarly, since anisotropy has been found to be an important parameter influencing pattern formation, Buka et al.⁶² have recently studied viscous fingering in liquid crystals.
- vi. In smectic films the two-dimensional hexatic phase has been found, and by increasing the number of layers, the cross-over to three dimensional behavior can be studied.⁶³
- vii. The nematic-smectic A transition is one that has been predicted to be weakly first order because of a coupling between director fluctuations and the smectic order parameter.⁶⁴ Since some experiments have failed to detect any measurable latent heat,^{65,66} and the correlation length of smectic A fluctuations in the nematic phase grows continuously as the transition is approached,⁶⁷ this prediction has remained somewhat controversial. Recently, however, even those samples that calorimetrically appear to have a second order transition, exhibited interfaces with all the static and dynamic signatures of a weakly first order transition. To our knowledge, this was the first time the order of a transition was inferred from interfacial properties.⁶⁸ Note also that in this experiment, interfaces between a stable and a metastable state are studied. The analysis of the interface velocity in such cases is closely related to the discussion in section 4.3.2.

Update: P.E. Cladis, J.T. Gleeson, P.L. Finn and H.R. Brand, [*Breathing Mode in a Pattern-Forming System with Two Competing Lengths*](#), Phys. Rev. Lett. **67**, (1991) where interfacial patterns at a traveling cholesteric (chiral)-isotropic liquid crystal interface find the converse of the Turing Instability (systems with a frequency can also have a length scale). the traveling cholesteric (which has a length scale)-isotropic interface has a frequency and a “route to turbulence”: H.R. Brand and P.E. Cladis, [*Nonequilibrium Phase Winding and its Breakdown at a Chiral Interface*](#), Phys. Rev. Lett. **72**, 104 (1994) *See also:* P.E. Cladis, [*Traveling Phase Boundaries with the Broken Symmetries of Life*](#), in *Chirality in Liquid Crystals*, H.-S. Kitzerow and C. Bahr (Eds.), Springer-Verlag, NY (2001) pp. 481-493.

4.5 Conclusions

In conclusion, liquid crystals are well suited as a tool to do nonlinear science: they are soft systems where nonlinearities are important. They are anisotropic systems and anisotropy influences macroscopic nonlinear behavior. Nonlinear dynamics in liquid crystals can be observed in real time and real space. In the long term, the study of liquid crystals provides a link with the many non-equilibrium and nonlinear problems of biology.

4.6 Afterward by PEC 4/16/06

Wim and I started working on this Chapter in 1989, just before the explosion of interest, led by Lorenz Kramer, Professor of Physics at the University of Bayreuth, in nonequilibrium problems in complex systems. We are profoundly indebted to Lorenz for his tireless energy dedicated to developing the field of nonequilibrium physics of complex materials, particularly liquid crystals, and deeply regret his untimely death.

NATO’s Special Program on Chaos, Order and Patterns sponsored a few of the many workshops that came out of his efforts. See for example:

1. *Nonlinear Evolution of Spatio-Temporal Structures in Dissipative Continuous Systems*, F.H. Busse and L. Kramer, Plenum Press, New York (1990).
2. *Pattern Formation in Complex Dissipative Systems: Fluid Patterns, Liquid Crystals and Chemical Reactions*, S. Kai (Ed.), World Scientific, Singapore (1991).
3. *Spatio-Temporal Patterns in Nonequilibrium Complex Systems*, P.E. Cladis and P. Palffy-Muhoray (Eds.), Proceedings Volume XXI in the Santa Fe Institute Studies in the Sciences of Complexity, Addison-Wesley Publishing Company, New York (1994).

CHAPTER FOUR REFERENCES

- [1] Lui Lam, *Mol. Cryst. Liq. Cryst.* 1/88. In this paper, Lam discusses how W. Little's exciton theory for high T_c materials may be realized by discotic or bowlic liquid crystals. *See also*: Superconductor Week, October 19, 1987, p.4.
- [2] H. R. Brand and Mauro Doria, (unpublished). In this paper, these authors discuss some consequences for a superconductor with a nematic-like order parameter.
- [3] P. E. Cladis, T. Garel and P. Pieranski, [Phys. Rev. Lett. 57, 2841 \(1986\)](#).
- [4] P. E. Cladis and M. Kleman, [J. de Physique 33, 591 \(1972\)](#).
- [5] *See for example*: P. E. Cladis, in *Dynamics and Defects in Liquid Crystal*, P.E. Cladis and P. Palffy-Muhoray (Eds.), Gordon and Breach Science Publishers, Canada (1998) p. 175ff, who shows that by escaping into the third dimension, a cholesteric helix may be completely unwound without introducing defects; P.E. Cladis, A. E. White and W. F. Brinkman, *J. Phys. (Paris)* **40**, 325 (1979), who show that, to minimize its elastic energy, an $S = 2$ defect with a core region that has escaped into the third dimension rotates with the opposite handedness to that given by the microscopic chirality.
- [6] P.E. Cladis, Y. Couder and H.R. Brand, [Phys. Rev. Lett. 55 2945 \(1985\)](#).
- [7] W. F. Brinkman and P. E. Cladis, [Physics Today 35, 48 \(1982\)](#).
- [8] P. E. Cladis, [Phys. Rev. Lett. 28, 1629 \(1972\)](#).
- [9] V. G. Kamenskii, *Sov. Phys. JETP* **60**, 723 (1984). (*Zh. Eksp. Teor. Fiz.* **87**, 1262 (1984)).
- [10] Frederick J. Almgren and Elliot H. Lieb, *Bull. Am. Math. Soc.*, **17**, 304 (1987). *Singularities of Energy Minimizing Maps from the Ball to the Sphere: Examples, Counterexamples, and Bounds* (submitted to *Annals of Mathematics*).
- [11] C. Williams, P. Pieranski and P. E. Cladis, [Phys. Rev. Lett. 29, 90 \(1972\)](#).
- [12] J. L. Ericksen in *Non-linear Effects in Fluids and Solids*, M.M. Carroll and M.A. Hayes Eds., Plenum, New York (1996) p. 137ff. (ASME Symposium, Rivlin Anniversary Volume (1988)).
- [13] P. E. Cladis, *Phil. Mag.* **29**, 641 (1974).

- [14] See e.g. *Solitons*, S. E. Trullinger, V. E. Zakharov and V. L. Prokovsky, Eds., North Holland, Amsterdam, (1986).
- [15] See e.g. M. Buttiker, in *Structure, Coherence and Chaos in Dynamical Systems*, P. L. Christiansen and R. D. Parmentier, Eds. (Manchester UP, Manchester, 1987); M. A. Collins, in *Advances in Chemical Physics*, Vol. **53** I. Prigogine and S. A. Rice, Eds., John Wiley and Sons, New York (1983).
- [16] F. Brochard, *J. de Physique*, **33**, 607 (1972).
- [17] See e.g. G. Dee and J. S. Langer, *Phys. Rev. Lett.* **50**, 383 (1983); E. Ben-Jacob, H. R. Brand, G. Dee, L. Kramer and J. S. Langer, *Physica* **41**, 348 (1985) and W. van Saarloos, *Phys. Rev.* **A37**, 211 (1988) and references therein. The first application of marginal stability to liquid crystals was made by Lin Lei, Shu Changqing and Xu Gang, *J. of Stat. Phys.*, **39**, 633 (1985).
- [18] A.C. Scott, *Neurophysics*, John Wiley and Sons, New York (1977); Xin-yi Wang (also Wang Xin -yi), *Phys. Lett.* **112A**, 402 (1985); *Phys. Rev.* **A32**, 3126 (1985).
- [19] P. E. Cladis, W. van Saarloos, P. L. Finn and A. R. Kortan, [Phys. Rev. Lett. 58, 222 \(1987\)](#).
- [20] G. N. Taylor and F. J. Kahn, *J. Appl. Phys.* **45**, 4330 (1974).
- [21] Elastic forces do not play a significant role in this initial re-orientation that takes place in a time of order $\gamma/\epsilon_a E^2$ with γ the appropriate combination of viscosities damping the splay-bend deformation. In the regime studied here, this is about a few milliseconds agreeing with the experimental observations.
- [22] This picture is supported by a more detailed stability analysis. To the left of the line defect, the director approaches the x-independent profile $\theta_0(y)$ given by Eq. 4.5. On substituting $\theta = \theta_0(y) + \delta\theta(y) \exp(-\omega t + kx)$, ($k > 0$), and linearizing, $\delta\theta$ is found to obey an equation of Schrödinger type with ω playing the role of the energy eigenvalue. With the use of arguments similar to those discussed by A.C. Scott, F.Y.F. Chu and D. W. McLaughlin, *Proc. IEEE* **61**, 1443 (1973), it can then be shown that $\omega > 0$, so the region to the left of the line is linearly stable.
- [23] As we discuss later, in the absence of fields, we have $F_{exc} \sim \ln(\ell)$ and Eq. 4.15 gives $\ell^2 \sim (t-t_0)$ for the annihilation of two defects.
- [24] The energy dissipation per unit time and line length is according to Ref. 23, $\int \gamma (\partial\theta/\partial t)^2 dx dy = c^2 \gamma \int (\partial\theta/\partial x)^2 dx dy$. Equating this to the change in elastic energy per unit time ($= cdF_{exc}/d\ell$) yields $b = 1/2 \int (\partial\theta/\partial x)^2 dx dy$. Using the expression for θ near a $1/2$ defect, $\theta =$

- $\phi/2$, gives $b = \frac{1}{2} \int_{r_c}^{\xi} dr [d\phi(\sin^2\phi)/4r = (\pi/8) \ln(\xi/r_c)]$, where r_c is the core size. From the formula after Eq. 4.10 we get $\xi \sim 6000\text{\AA}$ for $V = 50$ volts; taking $r_c = 28\text{\AA}$, we then get $b \sim 2.1$. This is expected to be an overestimate because the effect of the electric field is to decrease $(\partial\theta/\partial x)^2$ in the expression for b , and because the core size may be several molecular dimensions not just one.

- [25] K. Skarp, S. Lagerwall and B. Stebler, *Mol. Cryst. Liq. Cryst.* **60**, 215 (1980).
- [26] P. G. de Gennes, *The Physics of Liquid Crystals* (Oxford University Press, Oxford, 1974).
- [27] The field $\theta(y)$ in Eq. 4.10 away from the defect is a combination of splay and bend; the analysis leading to Eq. 4.14 can be extended to the case $K_1 \neq K_3$. For 5CB, the resulting correction is about 3%.
- [28] In this regard, we note that in [4.24] a larger value of the core size would give a lower estimate of b , e.g. $r_c = 60\text{\AA}$ gives $b \sim 1.8$.
- [29] Yu. A. Dreizin and A. M. Dykhne, *Zh. Eksp. Teor. Fiz.* **B 61** (1971) 2140 [*Sov. Phys. JETP B 34* (1972) 1140]
- [30] A.S. Sonin, A. N. Chuyrov, A. A. Sobachkin and V. L. Ovchinnikov, *Fiz. Tverd. Tela B 18* (1976) 3099 [*Sov. Phys. Solid State. B 18* (1976) 1805]
- [31] R. Pindak, C. Y. Young, R. B. Meyer and N. A. Clark, *Phys. Rev. Lett.* **45** (1980) 1193; see also Chapter 7 of this book.
- [32] P. E. Cladis, H. R. Brand and P. L. Finn, *Phys. Rev.* [A28, 512 \(1983\)](#). The name *helielectric* was first proposed in: H. R. Brand, P. E. Cladis and P. L. Finn, [Phys. Rev. A31 361 \(1985\)](#).
- [33] H. R. Brand and P. E. Cladis, [Mol. Cryst. Liq. Cryst. 114, 207 \(1984\)](#).
- [34] S. Kai, M. Nomiyama, T. Takahashi and M. Imasaki, *Japanese J. Appl. Phys.* **26** L1831 (1987).
- [35] N. A. Clark and S. T. Lagerwall, *Appl. Phys. Lett.* **36**, 899 (1980).
- [36] *See for example:* R. B. Meyer, *Mol. Cryst. Liq. Cryst.* **40**, 33 (1977).
- [37] M. Press and A. Arrott, *J. de Physique* **37**, 387 (1976).
- [38] D. G. Aronson and H. F. Weinberger, *Adv. Math.* **30**, 33 (1978).

- [39] J. E. Maclennan, M. A. Handschy and N. A. Clark, *Phys. Rev.* **A34**, 3554 (1986).
- [40] P. E. Cladis and W. van Saarloos (to be published).
- [41] B. D. Coleman (unpublished results) 1986.
- [42] *See e.g.* J. Geicke, *Phys. Lett.* **111A**, 10 (1985)
- [43] *See e.g.* J. Weiss, M. Tabor and G. Carnevale, *J. Math. Phys.* **24**, 522 (1983).
- [44] This way of obtaining an exact solution is similar to the one used by A. Saul and K. Showalter in *Oscillations and Traveling Waves in Chemical Systems*, R. J. Field and M. Burger, Eds. John Wiley and Sons, New York (1985).
- [45] J. L. Ericksen, *Kolloid-Z.* **173**, 117 (1960) and *Arch. Rat. Mech. Anal.* **4**, 231 (1960) *ibid* **89**, 371 (1962).
- [46] F. M. Leslie, *Q. J. Mech. Appl. Math.* \fB19\fR Pt.3-357 (1966).
- [47] O. Parodi, *J. de Physique*, **31**, 58 (1970). Parodi's relation, $\gamma_2 = \alpha_6 - \alpha_5 = \alpha_3 + \alpha_2$, is an Onsager relation for the Ericksen-Leslie stress tensor.
- [48] P. E. Cladis and S. Torza, [Phys. Rev. Lett.](#) **35**, 1283 (1975).
- [49] P. E. Cladis and S. Torza in *Colloid and Interface Science Vol.4*, M. Kelker (editor) Academic Press publishers, New York (1976) pp. 487-499.
- [50] P. C. Martin, O. Parodi and P. S. Pershan, *Phys. Rev.* **A6**, 2401 (1979).
- [51] H. R. Brand and H. Pleiner, *J. Physique* **41**, 553 (1980).
- [52] H. R. Brand and H. Pleiner, *J. de Physique*, **43**, 853 (1982).
- [53] S Diele, H. Hartung, P. Ebeling, D. Vettors, H. Kruger and D. Demus, in *Advances in Liquid Crystal Research and Applications*, edited by L. Bata (Pergamon Press, Oxford and Akademiai Kiado, Budapest, 1980), p.39.
- [54] J. J. Benattar, F. Moussa and M. Lambert, *J. Chim. Phys.* \fB80\fR, 99 (1983).
- [55] M. Abramowitz and I Stegun, *Handbook of Mathematical Functions*, Dover, New York, (1965), p. 375.
- [56] C. Y. Young, R. Pindak, N. A. Clark and R. B. Meyer, *Phys. Rev. Lett.* **40**, 773 (1978).

- [57] *See for example*: L. D. Landau and E. M. Lifshitz, *Fluid Mechanics*, Addison Wesley, Reading, Mass. (1959).
- [58] M. Lowe and J. P. Gollub, *Phys. Rev.* **A31**, 3893 (1985)
- [59] See W. van Saarloos and M. Grant, *Phys. Rev. B* **37**, 2274 (1988) for a more detailed discussion and references.
- [60] I. Rehburg, S Rasenat and V. Steinberg, *Phys. Rev. Lett.* **62**, 756 (1989). See also: W. Zimmermann, *MRS Bulletin* **16**, 38 (1991).
- [61] P. Oswald, J. Bechhoefer and A. Libchaber, *Phys. Rev.Lett.* **58**, 2318 (1987); P. Oswald, J. Bechhoefer, and F. Melo, *MRS Bulletin* **16** 38 (1991).
- [62] A. Buka, P. Palffy-Muhoray and Z. Racz, *Phys. Rev.* **A36** 3984 (1987); A. Buka and P. Palffy-Muhoray, *Phys. Rev.* **A36**, 1527 (1987) and S. Arora, A. Buka, P. Palffy-Muhoray, Z. Racz and R. Vora, *Europhys. Lett.* **7**, 43 (1988).
- [63] No systematic study has yet been made of this interesting possibility. However, E. B. Sirota, P. S. Pershan, L. B. Sorenson and J. Collet, *Phys. Rev. Lett.* **55**, 2039 (1985) found a continuous decrease as a function of temperature, in the correlation length between layers as the smectic G phase is approached through the smectic F phase. Far from the G phase, the layer correlation length is short range (about one layer thick) and is about the thickness of the film at the transition temperature. (see also Chapter 7.)
- [64] B. I. Halperin, T. C. Lubensky and S. K. Ma, *Phys. Rev. Lett.* **32**, 292 (1974) and B. I. Halperin and T. C. Lubensky, *Solid St. Comm*, **14**, 997 (1974).
- [65] M. A. Anisimov, V. P. Voronov, E. E. Gorodetskii, V. E. Podnek and F. Kholmudorov, *JETP Lett.* **45**, 425 (1987) [*Pisma. Zh. Eksp. Teor. Fiz.* **45**, 336 (1987)].
- [66] J. Thoen, H. Marynissen and H. van Dael, *Phys. Rev. Lett.* **52**, 204 (1984) and *Phys. Rev.* **A26**, 2886 (1982). H. Marynissen, J. Thoen and W. van Dael, *Mol. Cryst. Liq. Cryst.* **24**, 195 (1985).
- [67] B. M. Ocko, R. J. Birgeneau and J. D. Litster, *Z. Phys.* **62**, 487 (1986).
- [68] P. E. Cladis, W. van Saarloos, D. A. Huse, J. S. Patel, J. W. Goodby and P. L. Finn, [Phys. Rev. Lett.](#) **62**, 1764 (1989); M.A. Anisimov, P.E. Cladis, E.E. Gorodetskii, D.A. Huse, V.E. Podneks, V.G. Taratuta, W. van Saarloos and V.P. Voronov, [Phys. Rev. A](#) **41**, 6749 (1990); P.E. Cladis, *J. Stat. Phys.* **62**, 899 (1991).